

# Improved Constraints on the Acceleration History of the Universe and the Properties of the Dark Energy

Ruth A. Daly

*Department of Physics, Penn State University, Berks Campus, P. O. Box 7009, Reading,  
PA 19610*

rdaly@psu.edu

S. G. Djorgovski

*Division of Physics, Mathematics, and Astronomy, California Institute of Technology, MS  
105-24, Pasadena, CA 91125*

Kenneth A. Freeman, Matthew P. Mory

*Department of Physics, Penn State University, Berks Campus, P. O. Box 7009, Reading,  
PA 19610*

C. P. O'Dea, P. Kharb, & S. Baum

*Rochester Institute of Technology, 54 Lomb Memorial Drive, Rochester, NY 14623*

## ABSTRACT

We extend and apply a model-independent analysis method developed earlier by Daly & Djorgovski to new samples of supernova standard candles, radio galaxy and cluster standard rulers, and use it to constrain physical properties of the dark energy as functions of redshift. Similar results are obtained for the radio galaxy and supernova data sets, which rely upon completely independent methods, suggesting that systematic errors are relatively small for both types of distances; distances to SZ clusters show a scatter which cannot be explained by the quoted measurement errors. The first and second derivatives of the distance are compared directly with predictions in a standard model based on General Relativity. The good agreement indicates that General Relativity provides an accurate description of the data on look-back time scales of about ten billion years. The first and second derivatives are combined to obtain the acceleration parameter  $q(z)$ , assuming only the validity of the Robertson-Walker metric, independent of a theory of gravity and of the physical nature of the dark energy. The data are analyzed using a sliding window fit and using fits in independent

redshift bins. The acceleration of the universe at the current epoch is indicated by the sliding window fit analysis. The effect of non-zero space curvature on  $q(z)$  is explored; for a plausible range of values of  $\Omega_k$  the effect is small and causes  $a$  to shift to the redshift at which the universe transitions from deceleration to acceleration. We solve for the pressure, energy density, equation of state, and potential and kinetic energy of the dark energy as functions of redshift assuming that General Relativity is the correct theory of gravity. Results obtained using a sliding window fit indicate that a cosmological constant in a spatially flat universe provides a good description of each of these quantities over the redshift range from zero to about one. We define a new function, the dark energy indicator, in terms of the first and second derivatives of the coordinate distance and show how this can be used to measure deviations of  $w$  from  $-1$  and to obtain a new and independent measure of  $\Omega_m$ .

*Subject headings:* cosmological parameters - cosmology: observations - cosmology: theory - dark matter -equation of state

## 1. INTRODUCTION

Understanding of the physical nature of the dark energy which appears to be driving the accelerated expansion of the universe is among the most pressing and important topics in cosmology today. Studies of the expansion history of the universe allow us to constrain the physical nature of its matter and energy constituents. One way that the expansion and acceleration history of the universe can be studied is through the use of a set of coordinate distances and redshifts for some standard set of objects. Type Ia supernovae provide a modified standard candle (e.g. Phillips 1993, Hamuy et al. 1995) that allow the distance modulus, luminosity distance, and coordinate distance to each source to be determined. The recent data sets presented by Astier et al. (2006), Riess et al. (2007), Wood-Vasey et al. (2007), and Davis et al. (2007) have been analyzed by these groups and compared with numerous models by other researchers.

In a novel, largely model-independent approach to this problem, it was shown by Daly & Djorgovski (2003) that the first and second derivatives of the coordinate distance with respect to redshift could be obtained from the coordinate distances and combined to solve for the expansion rate  $H(z)/H_0$  and acceleration rate  $q(z)$  of the universe. The functions  $H(y')$  and  $q(y', y'')$  are exact, that is, they are not obtained by expansions in terms of derivatives about some point. The only assumptions are that the universe is described by a Robertson-Walker metric and has zero space curvature. The results are independent of the contents of the

universe and their physical properties, and even independent of whether General Relativity provides an accurate description of the universe. Here, we drop the assumption of zero space curvature; it turns out that the deceleration parameter at a redshift of zero,  $q_0$ , remains the same, independent of whether space curvature is zero or not.

In this paper we expand on the previous analysis done by Daly & Djorgovski (2003, 2004). First, we use updated and expanded data sets, as described in section 2.1. Second, we introduce a more direct way to compare the model-independent results obtained from the data with predictions; this is done by directly comparing the first and second derivatives of the coordinate distance with respect to redshift to predicted values in various models, as described in section 2.2. Third, we analyze the data using both a sliding window fit and fits in independent redshift bins. To solve for the physical properties of the dark energy as functions of redshift, a theory of gravity must be specified. To determine the properties of the dark energy, General Relativity is taken to be the correct theory of gravity, allowing us to solve for the pressure, energy density, and equation of state of the dark energy as a function of redshift in section 2.4. Fourth, in section 2.4, we introduce a way to solve for the potential and kinetic energy densities of the dark energy as functions of redshift. In addition, we define a new function, the dark energy indicator, which provides a measure of deviations of  $w$  from  $-1$  and a new and independent measure of  $\Omega_m$ . Fifth, in section 2.3, these derivatives are combined to solve for the expansion and acceleration rates of the universe as functions of redshift for both zero and non-zero space curvature; in our previous work we have not considered the effects of non-zero space curvature. The only assumption that must be made to obtain the functions  $H(z)/H_0$  and  $q(z)$  from the data are that the Robertson-Walker metric is valid in our universe. A discussion and conclusions follow in section 3.

## 2. DATA AND ANALYSIS

### 2.1. Data sets used

We consider three types of distances: those determined from luminosity distances to supernova standard candles (SN), those determined from the angular diameter distances to radio galaxies (RG), and those determined to clusters of galaxies with SZ measurements of angular diameter distances (CL).

The SN samples include those of Davis et al. (2007), Riess et al. (2007), and Astier et al. (2006); these authors provide the pertinent details about their measurements. There is some overlap between these supernovae samples, and this comparison allows the effects of

different samples and sub-samples to be seen. In addition, a comparison between the values of  $y(z)$ ,  $y'(z)$ , and  $y''(z)$  for the different samples goes hand in hand with a comparison of the best fit parameter values obtained in different models for these same samples, described by Daly et al. (2007). The 71 new supernovae presented by Astier et al. (2006) are included in both the Riess et al. (2007) and Davis et al. (2007) samples, and the high-redshift HST supernovae of Riess et al. (2007) are included in Davis et al. (2007) sample which, otherwise, includes only ESSENCE supernovae and low-redshift supernovae. These comparisons can be quite helpful, as illustrated by the work on Nesseris & Perivolaropoulos (2006).

The dimensionless coordinate distances  $y$  to supernovae can be obtained from the published distance moduli  $\mu$  using the best fit value of  $\kappa_{SN}$  and the relations  $\mu = \kappa_{SN} + 5\log_{10}[y(1+z)]$  and  $\sigma_y = y\sigma_\mu(\ln(10)/5)$ . There are several ways to determine  $\kappa_{SN} = 25 - 5\log_{10}(H_0/c)$  for published data sets that do not indicate the effective value of  $H_0$  adopted to obtain  $\mu$ ; the different methods provide values of  $\kappa_{SN}$  that are in good agreement. Here, we use the best fit value of  $\kappa_{SN}$  obtained by Daly et al. (2007). In the cases where a value of  $H_0$  is included in the publication of the values of  $\mu$  (e.g. Astier et al. 2006) the value of  $H_0$  adopted by Astier et al. (2006) is recovered to very high accuracy.

We use the new RG sample of Daly et al. (2007); eleven new radio galaxies were observed and analyzed, which increases the sample size to 30 radio galaxies with redshifts between zero and about 1.8.

Finally, we also use the angular diameter distances to a sample of 38 clusters determined with the SZ measurements by Bonamente et al. (2006). The angular diameter distances  $d_A$  obtained by Bonamente et al. (2006) for the hydrostatic equilibrium model were used. To convert from the angular diameter distance to the dimensionless coordinate distance we need to remove the value of  $H_0$  that was adopted by Bonamente et al. (2006), so we use their best fit value of  $H_0$  of  $76.9^{+3.9}_{-3.4}$  to obtain the dimensionless coordinate distance  $y$  to each of their clusters using the well-known relations  $d_A = (a_0 r)/(1+z)$  and  $y = (H_0/c)(a_0 r)$ .

After a detailed comparison between the SN and RG samples, we combine the Davis et al. (2007) supernovae sample with the Daly et al. (2007) radio galaxy sample, and study the combined sample of 222 sources. Dimensionless coordinate distances  $y$  and their uncertainties  $\sigma(y)$  are obtained for these samples as described by Daly et al. (2007), and are listed here in Table 1. We also study results obtained by adding the cluster sample of Bonamente et al. (2006) to obtain a sample of 260 sources, and these distances are also included in Table 1. Figure 1 shows a comparison of the distances for these three data sets relative to the standard Lambda Cold Dark Matter (LCDM) model with  $\Omega_m = 0.3$  and  $\Omega_\Lambda = 0.7$ . A comparison of each data set with the standard LCDM model indicates that both the SN and RG data sets provide reliable cosmology probes, while the SZ Cluster

method perhaps need some refinement; the reduced chi-square for the SN and RG is about one, as expected from the quoted measurement errors, whereas that for the SZ Clusters is greater than two, suggesting that the quoted errors substantially underestimate the true uncertainties of these distance measurements. However, to illustrate how our method can be applied to coordinate distances obtained using different methods, we consider the analysis of the full sample of 260 sources as well as the analysis of the sample of 222 SN and RG.

## 2.2. Determinations of $y'$ and $y''$

The distances  $y$  to each source are used to obtain the distance  $y(z)$  to any redshift within the redshift range of the sample, and first and second derivatives of the distance with respect to redshift,  $y'(z)$  and  $y''(z)$  and their uncertainties using the method of Daly & Djorgovski (2003, 2004).

In previous work, we have used  $y'$  and  $y''$  to obtain  $E(z) = H(z)/H_0$  and  $q(z)$ . We then compared our empirically determined functions  $E(z)$  and  $q(z)$  with predictions in different models. However, it is also possible to compare our empirically determined functions  $y'(z)$  and  $y''(z)$  directly with model predictions for these quantities. The predicted values of these quantities are labeled  $y'_p$  and  $y''_p$ .

For a universe with non-relativistic matter with mean mass energy density  $\Omega_m(1+z)^3$ , mean dark energy density  $\Omega_{DE}f(z)$ , and space curvature  $k$  in which Einstein's Equations apply, we have, in full generality, the predicted values of  $y'$ ,  $y'_p$ , and  $y''$ ,  $y''_p$  are given by

$$y'_p = \left( \frac{1 + \Omega_k y_p^2}{\Omega_m(1+z)^3 + \Omega_{DE}f(z) + \Omega_k(1+z)^2} \right)^{1/2} \quad (1)$$

and

$$y''_p = \frac{y'_p}{(1+z)} \left( \frac{\Omega_k y_p y'_p (1+z)}{(1 + \Omega_k y_p^2)} - 1.5 \frac{[\Omega_m(1+z)^3 + \Omega_{DE}(1+w)f(z) + (2/3)\Omega_k(1+z)^2]}{[\Omega_m(1+z)^3 + \Omega_{DE}f(z) + \Omega_k(1+z)^2]} \right) \quad (2)$$

where  $\Omega_k = -k/(H_0 a_0)^2$ ,  $\Omega_m = \rho_{0m}/\rho_{0c}$  is the zero redshift value of the mean mass density of non-relativistic matter relative to the critical density,  $\Omega_m + \Omega_{DE} + \Omega_k = 1$ , and  $y_p = \int_0^z y'_p dz$  is obtained by numerically integrating eq. (1). This derivation does not assume that  $w = P_{DE}/\rho_{DE}$ , is constant, and allows for variable  $w(z)$ . The function  $f(z)$  describes the redshift evolution of the energy density of the dark energy; in a quintessence model with constant equation of state  $w = P_{DE}/\rho_{DE}$ ,  $f(z) = (1+z)^{3(1+w)}$ , and for a cosmological constant  $f(z) = 1$ .

The data were analyzed using a sliding window fit, described in section 2.2.1, and using fits in independent redshift bins, described in section 2.2.2.

### 2.2.1. Results Obtained with a Sliding Window Fit

Fits are done using the window  $\Delta z = 0.6$  throughout for the SN data,  $\Delta z = 0.8$  for the RG data, when considered individually, and  $\Delta z = 0.6$  for the joint samples using the method described by Daly & Djorgovski (2003, 2004). The width of the fitting window is driven by the need to obtain useful confidence intervals for the fits by including a sufficient number of data points. As the size of the available data sets increases in the future, this width could be correspondingly narrowed. In decreasing the window function width from 0.6 to 0.5 and 0.4, the trends and overall results remain the same, the uncertainties increase (because there are fewer data points in the window), and the trends become more noisy (due to sparser sampling). In addition, to test whether the window function has an effect on the trends extracted from the data we created a mock data set with the same number and redshift distribution of points as in each data set and the same fractional error per point, but with  $y$  values obtained from a standard LCDM cosmology with  $\Omega_m = 0.3$  and  $\Omega_\Lambda = 0.7$  and ran it through the programs to extract  $y(z)$ ,  $y'(z)$ , and  $y''(z)$ . As expected, the uncertainties increase as the window width decreases due to the smaller number of data points in the window. For a window widths of 0.3 and 0.4 in redshift,  $y(z)$ ,  $y'(z)$ ,  $y''(z)$ , and  $q(z)$  match the input cosmology to very high precision. For widths of 0.5 and 0.6, there is a very slight offset of  $y''(z)$  and  $q(z)$  from the input cosmology that sets in above redshifts of about one, at a level that is very small compared with the uncertainties. Thus, the values of  $y(z)$ ,  $y'(z)$ ,  $y''(z)$ , and  $q(z)$ , and quantities obtained by combining these quantities, provide reliable determinations to redshifts well above one.

Our completely model-independent determinations of  $y(z)$ ,  $y'(z)$ , and  $y''(z)$  are shown in Figures 2 through 6. In Figures 2, 3, and 4, they are compared with the predicted value in a spatially flat universe, described by General Relativity with a cosmological constant  $\Omega_\Lambda = 0.7$ , and non-relativistic matter  $\Omega_m = 0.3$ . This provides a reasonable description of the data to redshift of about one or so for the supernovae and 1.5 or so for the radio galaxies. (We note that this is not a model fit, but simply an illustration of its compatibility with the data.)

The values of  $y'(z)$  and  $y''(z)$  obtained for the Davis et al. (2007) supernova sample are compared with the best fit model parameters obtained in a spatially flat quintessence model, a lambda model that allows for non-zero space curvature, and the standard LCDM model in Figures 5 and 6 using the best fit model parameters listed by Daly et al. (2007). The best

fit model parameters are obtained by fitting the data to a model, and each model is based upon General Relativity. A comparison of the first and second derivatives of  $y$  with those predicted in each of the models provides another way to see whether the model predictions provide a good description of the data. The models and best fit model parameters are shown for a lambda model that allows for non-zero space curvature, and a quintessence model.

Fig. 4 shows  $y''$  for each of the samples. The canonical LCDM model provides a good description of the radio galaxy data over the redshift range from zero to 1.5.

The comparison between the values of  $y'$  and  $y''$  determined directly from the data with those predicted in a standard LCDM model that relies upon the equations of General Relativity provides effectively a large-scale test of General Relativity. The good agreement obtained indicates that General Relativity provides a good description of the data on time scales (and the corresponding length scales) of about ten billion years.

For the Davis et al. (2007) sample of 192 supernovae, the best fit models track  $y'$  and  $y''$  to a redshift of about 1.2 or so, beyond which the data drops away from the model prediction (see Figs. 5 and 6). Curves expected for the best fit parameters obtained in a quintessence model and cosmological constant model with space curvature by fitting  $y(z)$ , obtained by Daly et al. (2007), are shown as well as a standard LCDM model. For  $y'$  all three curves fit well, and some differences emerge for  $y''$ ; in particular, the curve with non-zero space curvature does not fit the data well at low redshift.

### 2.2.2. Results Obtained With Fits in Independent Redshift Bins

Our sliding window fit method produces fit values which are strongly correlated over the redshift range corresponding to the fitting window, and are thus indicative of trends, but cannot be used simply to evaluate a statistical significance of any particular model. For that, we would need independent values at different redshifts. To this effect, we divided the data sample in a number of independent redshift bins (note: the data are *not* binned or averaged, the sample is divided in groups of points belonging to non-overlapping redshift bins). One drawback of this approach is that the numbers of data points in each bin are smaller, and thus the fit values are noisier. Another drawback is that the boundary values of the fits are not constrained, allowing for discontinuities in the values of  $y(z)$ ,  $y'(z)$ , and  $y''(z)$  at the bin boundaries, which physically makes no sense. This is the price of the statistical independence.

The dimensionless coordinate distances to the 192 supernovae of Davis et al. (2007) were combined with those to the 30 radio galaxies of Daly et al. (2007) to obtain a sample of

222 sources with redshift between 0.016 and 1.79. These data were divided into bins based on the redshifts of the points to be able to obtain independent determinations of  $y'$  and  $y''$  and their uncertainties. The data were divided into redshift bins with roughly equal numbers of points per bin. We considered 2 bins with 111 points each; 3 bins with 74 points each; 4 bins with 55 points in the first three bins and 57 points in the highest redshift bin; and 6 bins with 37 points each. The bin, number of points per bin, median redshift of the points in the bin, and the minimum and maximum redshift of points within the bin are listed in Table 2. Points in each bin were used to determine the values of  $y'$  and  $y''$  and their uncertainties at the median redshift of the bin.

The results for  $y'$  are shown in Figure 7 for 3, 4, and 6 bins; the redshift range of the points that went into the determination of  $y'$  at the median redshift  $z_{med}$  are indicated by the horizontal lines. Three theoretical curves are included on the figure. The dotted line is the curve predicted by the standard LCDM model with  $\Omega_m = 0.3$ , and the other two curves, which are nearly identical are those predicted in the Cardassian model (Freese & Lewis 2002) and the generalized Chaplygin gas model (Kamenshchik, Moschella, & Pasquier 2001; Bilic, Tupper, & Viollier 2002; and Bento, Bertolami, & Sen 2002) are shown for the best fit parameters obtained by Bento et al. (2005) assuming a spatially flat universe.

The results obtained for  $y''$  are shown in Figure 8 for 2 and 3 bins. The full set of results are listed in Table 2. Given the noise inherent in the data that is presently available, it is not possible to obtain meaningful results for  $y''$  with a larger number of independent bins. With more data, we will be able to obtain this quantity in a larger number of independent redshift bins.

### 2.3. Determinations of $H(z)/H_0$ and $q(z)$ for Zero Space Curvature

The dimensionless expansion rate  $E(z) \equiv H(z)/H_0$  and the deceleration parameter  $q(z)$  can be constructed directly from the first and second derivatives of the coordinate distance  $y'$  and  $y''$ , as discussed in detail by Daly & Djorgovski (2003). The relationship between  $E(z)$  and  $y'$ , and that between  $q(z)$  and  $y'$  and  $y''$  are exact; they do not represent expansions about some point. The only requirement to derive these exact relationships is that the most the Robertson-Walker line element applies in our universe. With this assumption alone, it can be shown that

$$H(z)/H_0 = (y')^{-1} (1 + \Omega_k y^2)^{1/2} \quad (3)$$

(e.g. Weinberg 1972), and

$$q(z) = -1 - (1 + z) y'' (y')^{-1} + \Omega_k y y' (1 + z) / (1 + \Omega_k y^2) \quad (4)$$



(Daly & Djorgovski 2003), where  $H(z)/H_0 \equiv (\dot{a}/a)^2$ ,  $q(z) \equiv -(\ddot{a}a)/(\dot{a})^2$ ,  $\Omega_k \equiv -k/(H_0 a_0)^2$ , and  $k$  is positive and  $\Omega_k$  is negative when space curvature is positive. Thus, the zero redshift value of  $q(z=0) = -1 - (y''/y')|_{z=0}$  is independent of space curvature, as is  $E_0 = (1/y')|_{z=0}$  since  $y = 0$  at  $z = 0$ . Thus, the zero redshift values of  $E(z)$  and  $q(z)$  obtained from  $y'$  and  $y''$  are independent of space curvature. And, the zero redshift value of  $q$  indicates whether the universe is accelerating at the current epoch and can be determined independent of  $\Omega_k$ .

### 2.3.1. Results Obtained with a Sliding Window Fit

The data and analysis described in section 2.2.1 were used to obtain  $H(z)/H_0$  and  $q(z)$  using equations 3 and 4. The results are shown in Figures 9 and 10 for the combined sample of 222 sources described above. The results confirm that the universe is accelerating at the current epoch. For the Davis et al. (2007) sample of 192 supernovae, we find a zero redshift value of  $q$  are  $q_0(192SN) = -0.48 \pm 0.11$ . For the radio galaxies, we find  $q_0(30RG) = -0.65 \pm 0.5$ , consistent with the results obtained using supernovae. Again, these results depend only upon the form of the Robertson-Walker line element and are independent of space curvature, whether General Relativity is the correct theory of gravity, and the content or evolution of the contents of the universe. For  $k = 0$ , the redshift at which the universe transitions from acceleration to deceleration for the Davis et al. (2007) sample of 192 SN  $z_T = 0.77 \pm 0.1$ .

We investigated the effect of the size of the window function of the value of  $q_0$  and the transition redshift for the combined sample of 192 supernovae and 30 radio galaxies. For a window function of width 0.6 in redshift, we obtain  $q_0 = -0.48 \pm 0.11$ , and a transition redshift  $z_T = 0.78_{-0.27}^{+0.08}$ ; for a window function of width 0.5 in redshift, we obtain  $q_0 = -0.37 \pm 0.13$ , and a transition redshift  $z_T = 0.79 \pm 0.15$ ; and for a window function of width 0.4, we obtain  $q_0 = -0.30 \pm 0.18$ , and  $z_T = 0.71 \pm 0.37$ . These numbers are all consistent, though the uncertainties increase as the size of the window function decreases since then fewer points are used to determine each quantity. It is important to increase the number of data points at all redshifts to that the size of the window function can be decreased. These transition redshifts are consistent with those obtained by Melchiorri, Pagano, & Pandolfi (2007).

### 2.3.2. Results Obtained With Fits in Independent Redshift Bins

The data and analysis described in section 2.2.2 were used to obtain  $H(z)/H_0$  and  $q(z)$  using equations 3 and 4. The results are shown in Figures 11 and 12, and are listed in Table 2.

The values of  $H(z_{med})$  are consistent with predictions in the standard LCDM model at about one sigma or better. For comparison, predictions obtained in a Cardassian model and generalized Chaplygin gas model, described in section 2.2.2. are also displayed. The value of the deceleration parameter at the median redshift of the bin,  $q(z_{med})$ , does not definitely show that the universe is accelerating today, using this approach. That is, we do not see that  $q$  must be less than zero. If we consider the data split into two bins, each with 111 data points, and review the results for the lower redshift bin, we find that at a redshift of 0.02 the value of  $q$  is  $-0.28 \pm 0.14$ . If we consider the data split into three bins, each with 74 data points, and review the results for the lowest redshift bin, we find that the value  $q$  is consistent with zero for all of the data points in this bin. Evidently, we do not yet have a sufficient density of data points even at a redshift less than about 0.5 to be able to definitely state at three sigma or better that the universe is accelerating today, using this method (fits in independent redshift bins). It is only when we increase the number of data points that go into the determination of  $q(z)$  by using the sliding window function, that we can conclude that the universe is accelerating today using our model-independent analysis.

Of course, when it is concluded that the universe is accelerating today in the context of a quintessence model or other models, all of the data are being used in the context of that particular model. The quintessence and most other models implicitly assume that our universe is described by the Robertson-Walker line element, the equations of General Relativity apply, and that a specific function for the redshift evolution of the dark energy is valid over the redshift interval under study. Much more data are needed in order to test independently these (perfectly reasonable) assumptions.

## 2.4. Determinations of the Properties of the Dark Energy

We can solve for the properties of the dark energy as functions of redshift if a theory of gravity is specified, as shown by Daly & Djorgovski (2004). Einstein's equations of General Relativity are used to relate the pressure,  $P_{DE}$ , energy density,  $\rho_{DE}$ , equation of state  $w = P_{DE}/\rho_{DE}$ , and potential,  $V_{DE}$  and kinetic  $K_{DE}$  energy densities as functions of redshift to the cosmic scale factor  $a$ , and the first and second derivatives of  $a$  with respect to time. Since the Robertson-Walker line element has been used to relate the first and second derivatives

of  $a$  with respect to time to the first and second derivatives of the coordinate distance with respect to redshift,  $y'$  and  $y''$ , the equations of General Relativity can be used to solve for the pressure, energy density, equation of state, and potential and kinetic energy density of the dark energy in terms of  $y'$  and  $y''$ , which are obtained directly from the data. Here a value of  $k = 0$  is assumed, and the equations of Daly & Djorgovski (2004) are used to solve for the properties of the dark energy as functions of redshift. To obtain the pressure, we only need to specify that Einstein's equations apply.

$$\frac{P_{DE}(z)}{\rho_{0c}} = -(y')^{-2}[1 + (2/3)(1+z) y'' (y')^{-1}] . \quad (5)$$

As pointed out by Daly & Djorgovski (2004), the zero redshift value of  $P$  translates into a value of  $\Omega_\Lambda$  is a standard LCDM model since in this model  $w = -1$ , so  $\Omega_\Lambda = \rho_{DE}/\rho_{0c} = -P_0/\rho_{0c}$ . Here, this implies that  $\Omega_\Lambda = 0.64 \pm 0.1$  if the dark energy is due to a cosmological constant in a universe with zero space curvature. This value of  $\Omega_\Lambda$ , which is obtained from the first and second derivatives of the coordinate distance, is consistent with other measures.

To obtain the energy density  $\rho_{DE}$  of the dark energy,  $\Omega_m$  must be specified, and a value of  $\Omega_m = 0.3$  is adopted here.

$$\frac{\rho_{DE}(z)}{\rho_{0c}} = (y')^{-2} - \Omega_m(1+z)^3 . \quad (6)$$

The equation of state  $w$  is obtained by taking the ratio  $P_{DE}/\rho_{DE}$  and is given by

$$w(z) = \frac{-[1 + (2/3)(1+z) y'' (y')^{-1}]}{1 - \Omega_m(1+z)^3 (y')^2} . \quad (7)$$

The potential energy density of a dark energy scalar field is given by  $V = 0.5(\rho - P)$  so

$$\frac{V_{DE}(z)}{\rho_{0c}} = (y')^{-2}[1 + (1+z)y''/(3y')] - 0.5\Omega_m(1+z)^3 \quad (8)$$

and the kinetic energy density is given by  $K = 0.5(\rho + P)$  so

$$\frac{K_{DE}}{\rho_{0c}} = -y''(1+z)/[3(y')^3] - 0.5\Omega_m(1+z)^3 , \quad (9)$$

since  $V = 0.5(\rho - P)$  and  $K = 0.5(\rho + P)$ .

We define a new function, the dark energy indicator  $s$ , which is given by

$$s = \frac{y''}{(y')^3(1+z)^2} . \quad (10)$$

This is motivated by the fact that, for zero space curvature, the predicted value of  $s$  is

$$s_p = -1.5\Omega_m \left( 1 + [1 + w] \frac{\Omega_{DE} f(z)}{\Omega_m [1 + z]^3} \right) = -1.5\Omega_m \left( 1 + [1 + w] \frac{\rho_{DE}}{\rho_m} \right) \quad (11)$$

as indicated by equations (1) and (2); this occurs because  $y_p'' \propto (y_p')^3(1+z)^2$  when  $\Omega_k = 0$ . Equation 11 is derived assuming only that General Relativity is valid, space curvature is zero, and there are two mass-energy components controlling the expansion of the universe, dark energy and non-relativistic matter including dark matter and baryons. It is not assumed that the equation of state of the dark energy,  $w$ , is constant, and no functional form for the evolution of the energy density of the dark energy,  $f(z)$ , is assumed. If  $w = -1$ , then  $s_p = -1.5\Omega_m$ , and the value of  $s$  provides a new and independent measure of  $\Omega_m$ . Deviations of  $s$  from a constant provide a measure of the deviations of  $w$  from -1; the amount of the deviation also depends upon the ratio of the energy density of the dark energy  $\rho_{DE}(z)$  to that of the mass density of non-relativistic matter  $\rho_m(z)$ , including dark matter and baryons, at a given redshift as discussed in more detail below.

#### 2.4.1. Results Obtained with a sliding window fit

The analysis described in section 2.2.1 was applied to the combined sample of 192 supernovae from Davis et al. (2007) and 30 radio galaxies from Daly et al. (2007). The values of  $y'$  and  $y''$  were substituted into equations 5, 6, 7, 8, 9, 10, and 15 and the results are shown in Figures 13, 14, 10, and 15. The zero redshift values of these parameters are  $P_0/\rho_{0c} = -0.64 \pm 0.10$ ,  $\rho_{DE}(z=0)/\rho_{0c} = 0.67 \pm 0.05$ ,  $w_0 = -0.95 \pm 0.08$ ,  $V_0/\rho_{0c} = 0.65 \pm 0.05$ ,  $K_0/\rho_{0c} = 0.01 \pm 0.03$ , and  $s_0 = -0.50 \pm 0.08$ . The zero redshift value of  $s$  indicates a value of  $\Omega_m = 0.33 \pm 0.05$  if  $w = -1$ , and the zero redshift value of  $P$  indicates a value of  $\Omega_\Lambda = 0.64 \pm 0.10$  if  $w = -1$ . Overall, the results are consistent with predictions in a standard LCDM model.

As noted above, the dark energy indicator  $s$  provides a measure of whether  $w = -1$  over the redshift range shown in Figure 15. To illustrate the signature of a value of  $w$  that differs from  $-1$ , three curves are overlaid on the figure. Each curve is obtained using equation 11 assuming  $\Omega_m = 0.3$ ,  $\Omega_{DE} = 0.7$ ,  $f(z) = 1$  and  $w$  is constant over the redshift range shown, with values of  $w$  of  $-1.2$  (short dashed curve),  $w = -1$  (solid line), and  $w = -0.8$  (long dashed curve). Clearly, the curves with  $w = -0.8$  and  $w = -1.2$  do not provide a good description of the data. Another way to look at this is that equation 10 and 11 indicate that  $w = -1 - (\rho_m/\rho_{DE})[2s/(3\Omega_m) + 1]$  so the second part of this is a measure of the deviation of  $w$  from -1, and at zero redshift the ratio  $\rho_m/\rho_{DE} \sim 0.3/0.7$  and  $\Omega_m = 0.3$ , so  $s$  places rather strong constraints on deviations of  $w_0$  from -1.

Since most of these functions involve combinations of the first and second derivatives of the coordinate distance, results obtained with independent redshift bins are quite noisy, so only values obtained in two independent redshift bins are listed in Table 3.

### 2.5. Effect of Space Curvature on $H(z)/H_0$ and $q(z)$

Space curvature, parameterized by  $\Omega_k$ , has only a modest effect on  $q(z)$ , as illustrated in Figure 17. Positive space curvature, with negative  $\Omega_k$  flattens the  $q(z)$  curve and pushes the redshift at which the universe transitions from an accelerating state to a decelerating state to higher redshift. This follows since  $y'$  is known to be positive in our universe since the universe is expanding. Similarly, negative space curvature moves the redshift at which  $q = 0$  to lower redshift causing the universe the transition from an accelerating to a decelerating state at lower redshift. For  $k = 0$ , the redshift at which the universe transitions from acceleration to deceleration for the Davis et al. (2007) sample is  $z_T = 0.77^{+0.11}_{-0.24}$ . For negative space curvature with  $\Omega_k = 0.1$  this transition redshift is shifted to about 0.6, and for positive space curvature with  $\Omega_k = -0.1$  it shifts to about 0.8.

Space curvature also affects the shape of  $H(z)/H_0$  as illustrated in Figure 16. Positive values of  $\Omega_k$  cause  $H(z)$  to increase more steeply with redshift than negative values of  $\Omega_k$ , which tend to flatten out the  $H(z)$  curve.

Thus, the effect of space curvature on  $H(z)$  and  $q(z)$  is small relative to the overall uncertainties of their measurements, within a plausible range of the curvature parameter  $\Omega_k$ .

### 2.6. Determinations of $y'$ and $y''$ for other samples

We also consider the full sample of 260 sources including the 38 SZ clusters of Bonamente et al. (2006), the 192 supernovae of Davis et al. (2007), and the 30 radio galaxies of Daly et al. (2007). These results are shown in Figure 18; a window function of width 0.6 was used to analyze the data. This analysis illustrates how this method can be applied to diverse data sets. However, while the SZ cluster distances currently provide a useful tool for measurements of the far-field Hubble parameter, it is probably premature to use them as standard rulers to probe the global geometry and kinematics of the universe at this time.

Gamma-ray bursts as standard candles have been analyzed in detail by Schaefer (2007), who gives other pertinent references. The values of  $\mu$  listed by Schaefer (2007) can be used to determine the dimensionless coordinate distance to each source if the value of  $H_0$  relevant for the sample is known, as described in section 2.1, and a value of  $H_0 = 70 \text{ km s}^{-1} \text{ Mpc}^{-1}$

was used (Schaefer, private communication). The dimensionless coordinate distances were analyzed to determine the functions  $y(z)$ ,  $y'(z)$ , and  $y''(z)$  using a window function of width 2.0 in redshift. A first look at results for the gamma-ray bursts are shown in Fig. 19, which suggest that these are a potentially promising tool to study cosmology at very large distances, and are broadly consistent with predictions in the canonical LCDM model, but the quality and the sparsity of the data are still not sufficient for the model-independent analysis as shown above for the SN+RG sample.

### 3. SUMMARY AND CONCLUSIONS

The work presented here improves and extends our previous results. First, expanded and improved data sets are considered: three supernova samples and one radio galaxy sample. The radio galaxy data set has 11 new sources, increasing its size to 30 sources, and the supernovae data sets have increased substantially in size and quality. In addition, SZ cluster distances and gamma-ray burst distances are considered. The dimensionless coordinate distances (obtained directly from the data), and first and second derivatives of the distance are obtained as functions of redshift using a sliding window fit. The good agreement obtained using supernovae and radio galaxies, two completely independent methods, with sources that cover similar redshift ranges, suggests that neither method is strongly affected by systematic effects, and that each method provides a reliable cosmological tool.

The first and second derivatives of the distance are combined to obtain the acceleration parameter  $q(z)$ , allowing for non-zero space curvature. It is shown that the zero redshift value of  $q(z)$ ,  $q_0$ , is independent of space curvature, and can be obtained from the first and second derivatives of the coordinate distance. Thus,  $q_0$ , which indicates whether the universe is accelerating at the current epoch, can be obtained directly from the supernova and radio galaxy data; our determinations of  $q(z)$  only relies upon the validity of the Robertson-Walker line element, and is independent of a theory of gravity, and the contents of the universe. Each of the supernova samples, analyzed using a sliding window fit, indicate that the universe is accelerating today independent of space curvature, independent of whether General Relativity is the correct theory of gravity, and of the contents of the universe. The effect of non-zero space curvature on  $q(z)$  is to shift the redshift at which the universe transitions from acceleration to deceleration, moving this to lower redshift for negative space curvature and to higher redshift for positive space. The zero redshift values of  $q$  obtained using a sliding window fit. for the Davis et al. (2007) supernova sample is  $q_0(192SN) = -0.48 \pm 0.11$  and that obtained for the radio galaxy sample of Daly et al. (2007) is  $q_0(30RG) = -0.65 \pm 0.53$  indicating that the universe is accelerating at the current epoch. The data were also binned

so that only certain subsets of the data were used to solve for  $y'$ ,  $y''$ ,  $H(z)/H_0$ , and  $q(z)$ . The results for  $y'$  and  $H(z)/H_0$  indicate that the standard LCDM model provides a good description of the data. The results for  $y''$  and  $q(z)$  are consistent with the standard LCDM model, but do not independently confirm the model or the acceleration of the universe.

In addition to the evaluation of the standard cosmological parameters, in an even more direct approach, we compared  $y'$  and  $y''$  obtained from the fits to the data to model predictions. Comparisons of  $y'$  and  $y''$  with predictions based on General Relativity indicate that General Relativity provides an accurate description of the data on look-back time scales of about ten billion years, thus providing a very large scale test of General Relativity.

Another new approach is that the data were analyzed using both a sliding window fit and fits in independent redshift bins. The fits in statistically independent redshift bins are broadly consistent with the sliding window fits, but are generally noisier (as expected).

We also explored the effects of non-zero space curvature on determinations of  $H(z)$  and  $q(z)$ . It is shown that the zero redshift value of  $q$ , obtained by applying equation (4) to  $y'$  and  $y''$ , is independent of space curvature. This means that our method can be used to determine  $q_0$ , and thus the degree to which the universe is accelerating at the current epoch, with only one assumption, that the Robertson-Walker line element is valid. In addition, it is found that the effect of space curvature on the shape of  $H(z)$  and  $q(z)$  is small, relative to the uncertainties arising from the measurement errors.

After determining the expansion and acceleration rates of the universe as functions of redshift independent of a theory of gravity, we solve for the pressure, energy density, equation of state, and potential and kinetic energy of the dark energy as functions of redshift assuming that General Relativity is the correct theory of gravity. We also define a new function, the dark energy indicator  $s$ , which provides a measure of deviations of the equation of state of the dark energy  $w$  from  $-1$ , and provides a new and independent measure of  $\Omega_m$  if  $w = -1$ . The results obtained using a sliding window fit indicate that a cosmological constant in a spatially flat universe provides a good description of each of these quantities over the redshift range from zero to one. The zero redshift values of these quantities obtained with the Davis et al. (2007) supernovae sample are  $P_{DE,0}/\rho_{0c} = -0.64 \pm 0.10$ ,  $\rho_{DE,0}/\rho_{0c} = 0.67 \pm 0.05$ ,  $w_{DE,0} = -0.95 \pm 0.08$ ,  $V_{DE,0}/\rho_{0c} = 0.65 \pm 0.05$ ,  $K_{DE,0}/\rho_{0c} = 0.01 \pm 0.03$ , and  $s_0 = -0.50 \pm 0.08$ . In the standard Lambda-Cold Dark Matter Model,  $\Omega_\Lambda = -P_0/\rho_{0c} = 0.64 \pm 0.1$ , obtained using the first and second derivatives of the coordinate distance, provides an independent measure of  $\Omega_\Lambda$ . In addition, in this model,  $w = -1$ , so  $s$  provides a measure of  $\Omega_m$ , and the value obtained here using the first and second derivatives of the coordinate distance, is  $\Omega_m = 0.33 \pm 0.05$ . Overall, the shapes of the pressure, energy density, equation of state, and other parameters as functions are redshift are consistent with those predicted in a standard

ΛCDM model. There is a tantalizing hint that there may be deviations from the standard model at high redshift; more observations at high redshift will be needed to investigate this further. The results obtained using fits in independent redshift bins are consistent with the standard ΛCDM model, but do not independently confirm the model.

We would like to thank the observers for their tireless efforts in obtaining the data used for this study. We would also like to thank the referee for helpful comments and suggestions. This work was supported in part by U. S. National Science Foundation grants AST-0507465 (R.A.D.) and AST-0407448 (S.G.D.), and the Ajax Foundation (S.G.D.).

## REFERENCES

- Astier, P., Guy, J., Regnault, N., Pain, R., Aubourg, E., Balam, D., Basa, S., Carlberg, R. G., Fabbro, S., Fouchez, D., and 32 coauthors, 2006, *A&A*, 447, 31
- Bento, M. C., Bertolami, O., Santos, N. M. C., & Sen, A. A. 2005, *astro-ph/0512076*
- Bento, M. C., Bertolami, O., & Sen, A. A. 2002, *Phys. Rev. D*, 66, 043507
- Bilic, N., Tupper, G. B., & Viollier, R. D. 2002, *Phys. Lett. B*, 535, 17
- Bonamente, M., Joy, M. K., LaRoque, S. J., Carlstrom, J. E., Reese, E. D., & Dawson, K. S. 2006, *ApJ*, 647,25
- Daly, R. A., & Djorgovski, S. G. 2003, *ApJ*, 597, 9
- Daly, R. A., & Djorgovski, S. G. 2004, *ApJ*, 612, 652
- Daly, R. A., Mory, M. P., O’Dea C. P., Kharb, P., Baum, S., Guerra, E. J., & Djorgovski, S. G. 2007, in press (*astro-ph 0710.5112*)
- Davis, T. M., Mortsell, E., Sollerman, J., Becker, A. C., Blondin, S., Challis, P., Clocchiatti, A., Filippenko, A. V., Foley, R. J., Garnavich, P. M., and 17 coauthors, submitted to *ApJ*, (*astro-ph/0701510*)
- Freese, K., & Lewis, M. 2002, *Phys. Lett. B*, 540, 1
- Hamuy, M., Phillips, M. M., Maza, J., Suntzeff, N. B., Schommer, R. A., & Aviles, R. 1995, *AJ*, 109, 1
- Kamenshchik, A. Y., Moschella, U., & Pasquier, V. 2001, *Phys. Lett. B*, 511, 265
- Kharb, P., O’Dea, C. P., Baum, S. A., Daly, R., Mory, M., Donahue, M., & Guerra, E., 2007, *ApJ*, in press
- Melchiorri, A., Pagano, L., & Pandolfi, S. 2007, *astro-ph/07061314*



- Nesseris, S., & Perivolaropoulos, L. 2006, astro-ph/0612653
- O’Dea, C. P., Daly, R., Kharb, P., Freeman, K. A., & Baum, S. A., 2007, ApJ, submitted
- Perlmutter, S., et al. 1999, ApJ, 517, 565
- Phillips, M. M. 1993, ApJ, 413, L105
- Riess, A. G., et al. 1998, AJ, 116, 1009
- Riess, A. G., Strolger, L. G., Casertano, S., Ferguson, H. C., Mobasher, B., Gold, B., Challis, P. J., Filippenko, A. V., Jha, S., Li, W., and 11 co-authors, 2007, ApJ, 659, 98
- Schaefer, B. E., ApJ, 660, 16.
- Weinberg, S. 1972, Gravitation and Cosmology, (New York: Wiley)
- Wood-Vasey, W. M., Miknaitis, G., Stubbs, C. W., Jha, S., Riess, A. G., Garnavich, P. M., Kirshner, R. P., Aguilera, C., Becker, A. C., Blackman, J. W., and 27 co-authors, submitted (astro-ph/0701041)

Table 1. Distances 192 Supernovae, 30 Radio Galaxies, and 38 Galaxy Clusters

Type	Source	$z$	$y$	$\sigma_y$
SN	sn1994S	0.016	0.0160	0.0016
SN	sn2001V	0.016	0.0145	0.0015
SN	sn1996bo	0.016	0.0135	0.0015
SN	sn2001cz	0.016	0.0155	0.0017
SN	sn2000dk	0.016	0.0161	0.0016
SN	sn1997Y	0.017	0.0174	0.0018
SN	sn1998ef	0.017	0.0146	0.0016
SN	sn1998V	0.017	0.0160	0.0016
SN	sn1999ek	0.018	0.0155	0.0016
SN	sn1992bo	0.018	0.0190	0.0018
SN	sn1992bc	0.020	0.0200	0.0017
SN	sn2000fa	0.022	0.0205	0.0020
SN	sn1995ak	0.022	0.0187	0.0018
SN	sn2000cn	0.023	0.0226	0.0019
SN	sn1998eg	0.024	0.0248	0.0023
SN	sn1994M	0.024	0.0239	0.0022
SN	sn2000ca	0.025	0.0239	0.0019
SN	sn1993H	0.025	0.0224	0.0019
SN	sn1992ag	0.026	0.0228	0.0023
SN	sn1999gp	0.026	0.0284	0.0021
SN	sn1992P	0.026	0.0281	0.0025
SN	sn1996C	0.028	0.0329	0.0027
SN	sn1998ab	0.028	0.0231	0.0019
SN	sn1997dg	0.030	0.0361	0.0032
SN	sn2001ba	0.031	0.0319	0.0023
SN	sn1990O	0.031	0.0309	0.0024
SN	sn1999cc	0.032	0.0310	0.0024
SN	sn1996bl	0.035	0.0350	0.0029
SN	sn1994T	0.036	0.0338	0.0026
SN	sn2000cf	0.037	0.0395	0.0031
SN	sn1999aw	0.039	0.0429	0.0026

Table 1—Continued

Type	Source	$z$	$y$	$\sigma_y$
SN	sn1992bl	0.043	0.0417	0.0035
SN	sn1992bh	0.045	0.0505	0.0044
SN	sn1995ac	0.049	0.0431	0.0032
SN	sn1993ag	0.050	0.0541	0.0045
SN	sn1990af	0.050	0.0454	0.0042
SN	sn1993O	0.052	0.0553	0.0038
SN	sn1998dx	0.054	0.0503	0.0035
RG	3C 405	0.056	0.0514	0.0105
SN	sn1992bs	0.063	0.0695	0.0064
SN	sn1993B	0.071	0.0736	0.0064
SN	sn1992ae	0.075	0.0713	0.0069
SN	sn1992bp	0.079	0.0731	0.0050
SN	sn1992br	0.088	0.0718	0.0076
SN	sn1992aq	0.101	0.1145	0.0079
SN	sn1996ab	0.124	0.1174	0.0108
CL	Abell 1413	0.142	0.2283	0.0454
CL	Abell 2204	0.152	0.1801	0.0192
SN	e020	0.159	0.1716	0.0229
CL	Abell 2259	0.164	0.1731	0.0806
CL	Abell 586	0.171	0.1561	0.0405
CL	Abell 1914	0.171	0.1321	0.0135
CL	Abell 2218	0.176	0.1990	0.0377
SN	k429	0.181	0.1764	0.0138
CL	Abell 665	0.182	0.2000	0.0288
CL	Abell 1689	0.183	0.1971	0.0273
CL	Abell 2163	0.202	0.1602	0.0139
SN	d086	0.205	0.1887	0.0261
SN	h363	0.213	0.2103	0.0320
SN	n404	0.216	0.2364	0.0338
CL	Abell 773	0.217	0.3057	0.0484
SN	g005	0.218	0.2133	0.0255

Table 1—Continued

Type	Source	$z$	$y$	$\sigma_y$
CL	Abell 2261	0.224	0.2290	0.0518
CL	Abell 2111	0.229	0.2016	0.0583
CL	Abell 267	0.230	0.1892	0.0315
CL	RX J2129.7+0005	0.235	0.1456	0.0301
SN	e132	0.239	0.2146	0.0287
CL	Abell 1835	0.252	0.3434	0.0160
CL	Abell 68	0.255	0.2027	0.0563
SN	04D3ez	0.263	0.2462	0.0238
SN	n326	0.268	0.2509	0.0300
SN	k425	0.274	0.2881	0.0371
CL	Abell 697	0.282	0.2892	0.0871
SN	p455	0.284	0.2832	0.0378
SN	03D4ag	0.285	0.2678	0.0160
SN	m027	0.286	0.3447	0.0508
CL	Abell 611	0.288	0.2575	0.0594
CL	ZW 3146	0.291	0.2747	0.0066
SN	03D3ba	0.291	0.2196	0.0324
SN	g055	0.302	0.3192	0.0544
SN	d117	0.309	0.3219	0.0400
SN	n278	0.309	0.2856	0.0276
CL	Abell 1995	0.322	0.4033	0.0491
CL	MS 1358.4+6245	0.327	0.3844	0.0323
SN	03D1fc	0.331	0.2996	0.0290
SN	e029	0.332	0.3297	0.0425
SN	d083	0.333	0.2279	0.0147
SN	04D3kr	0.337	0.3209	0.0251
SN	g097	0.340	0.3354	0.0479
SN	04D3nh	0.340	0.3463	0.0271
SN	m193	0.341	0.2960	0.0313
SN	d149	0.342	0.3459	0.0334
SN	h364	0.344	0.2994	0.0234

Table 1—Continued

Type	Source	$z$	$y$	$\sigma_y$
SN	03D1bp	0.346	0.3248	0.0374
SN	h359	0.348	0.3881	0.0483
SN	e136	0.352	0.3417	0.0425
SN	04D2fs	0.357	0.3452	0.0350
SN	04D3fk	0.358	0.3089	0.0299
SN	d093	0.363	0.3566	0.0230
SN	n263	0.368	0.3285	0.0257
SN	03D3ay	0.371	0.3662	0.0388
CL	Abell 370	0.375	0.3807	0.0687
SN	g052	0.383	0.3250	0.0329
SN	g142	0.399	0.3862	0.0765
SN	d085	0.401	0.3857	0.0391
SN	k448	0.401	0.4594	0.0846
RG	3C142.1	0.406	0.3325	0.0607
CL	MACS J2228.5+2036	0.412	0.4416	0.0851
SN	04D2fp	0.415	0.3999	0.0313
SN	k485	0.416	0.4184	0.0751
SN	g133	0.421	0.4286	0.0651
SN	h342	0.421	0.4208	0.0310
SN	f235	0.422	0.3498	0.0387
SN	b013	0.426	0.3824	0.0405
SN	e148	0.429	0.4321	0.0398
SN	04D2gb	0.430	0.3526	0.0292
RG	3C 244.1	0.430	0.3631	0.0671
SN	d089	0.436	0.3922	0.0361
SN	d097	0.436	0.4013	0.0314
SN	03D3aw	0.449	0.3923	0.0434
CL	RX J1347.5-1145	0.451	0.3571	0.0260
SN	04D3gt	0.451	0.2812	0.0298
SN	HST04Yow	0.460	0.4114	0.0625
SN	03D3cd	0.461	0.3982	0.0330

Table 1—Continued

Type	Source	$z$	$y$	$\sigma_y$
SN	03D3cc	0.463	0.4222	0.0331
SN	m158	0.463	0.4914	0.0634
SN	e108	0.469	0.4262	0.0314
SN	04D3df	0.470	0.3796	0.0350
SN	sn2002dc	0.475	0.4091	0.0396
CL	MACS J2214.9-1359	0.483	0.5474	0.0950
CL	MACS J1311.0-0310	0.490	0.5271	0.1604
SN	g160	0.493	0.4391	0.0526
SN	h319	0.495	0.4426	0.0428
SN	03D1ax	0.496	0.4283	0.0394
SN	e149	0.497	0.4087	0.0489
SN	h283	0.502	0.4592	0.0782
SN	03D1au	0.504	0.4713	0.0391
SN	p524	0.508	0.4449	0.0451
SN	g120	0.510	0.4185	0.0405
SN	d084	0.519	0.5612	0.0749
RG	3C172	0.519	0.6635	0.1366
SN	04D2gc	0.521	0.4431	0.0673
SN	04D1ak	0.526	0.4520	0.0604
SN	n285	0.528	0.4814	0.0576
SN	d033	0.531	0.5594	0.0438
SN	03D3af	0.532	0.5289	0.0706
SN	f011	0.539	0.4846	0.0558
SN	f244	0.540	0.4979	0.0596
CL	CL 0016+1609	0.541	0.5451	0.0869
CL	MACS J1149.5+2223	0.544	0.3166	0.0693
CL	MACS J1423.8+2404	0.545	0.5901	0.0178
RG	3C 330	0.549	0.3424	0.0652
CL	MS 0451.6-0305	0.550	0.5642	0.0973
SN	04D4bq	0.550	0.5016	0.0670
SN	04D3hn	0.552	0.4035	0.0762

Table 1—Continued

Type	Source	$z$	$y$	$\sigma_y$
SN	f041	0.561	0.4912	0.0385
CL	MACS J2129.4-0741	0.570	0.5352	0.1308
SN	03D4gf	0.581	0.5149	0.0427
SN	03D1aw	0.582	0.5828	0.0564
CL	MS 2053.7-0449	0.583	1.0063	0.1725
CL	MACS J0647.7+7015	0.584	0.3126	0.0792
SN	03D4gg	0.592	0.5161	0.0594
SN	h323	0.603	0.5467	0.0554
SN	03D4dy	0.604	0.4937	0.0728
SN	04D3do	0.610	0.4987	0.0666
SN	e138	0.612	0.5386	0.0446
SN	04D4an	0.613	0.5611	0.1008
SN	f231	0.619	0.5513	0.0432
SN	04D3co	0.620	0.5904	0.0707
SN	03D4dh	0.627	0.5216	0.0552
RG	3C 337	0.630	0.5064	0.0704
SN	e140	0.631	0.5084	0.0421
SN	n256	0.631	0.5575	0.0385
SN	g050	0.633	0.4805	0.0398
SN	03D4at	0.633	0.6021	0.0693
RG	3C169.1	0.633	0.6222	0.0708
SN	sn2003be	0.640	0.5246	0.0628
SN	04D3cy	0.643	0.6209	0.0629
SN	e147	0.645	0.5327	0.0442
RG	3C44	0.660	0.7621	0.0848
SN	sn2003bd	0.670	0.5597	0.0644
SN	03D1co	0.679	0.6817	0.0848
CL	MACS J0744.8+3927	0.686	0.7261	0.1858
SN	g240	0.687	0.5267	0.0485
SN	h300	0.687	0.5390	0.0422
SN	03D1fl	0.688	0.5486	0.0581

Table 1—Continued

Type	Source	$z$	$y$	$\sigma_y$
RG	3C34	0.690	0.5920	0.0644
SN	04D2iu	0.691	0.6259	0.1124
SN	p454	0.695	0.6569	0.0514
SN	03D4cz	0.695	0.5414	0.0848
RG	3C441	0.707	0.5340	0.0667
SN	04D3is	0.710	0.7074	0.1108
RG	3C 55	0.720	0.5852	0.0777
SN	04D1aj	0.721	0.6264	0.0664
SN	04D3fq	0.730	0.6556	0.0785
SN	sn2002kd	0.735	0.5265	0.0485
SN	HST04Rak	0.740	0.5863	0.0621
SN	04D2ja	0.741	0.6544	0.0723
RG	3C 247	0.749	0.5430	0.0682
SN	04D3ks	0.752	0.5877	0.0622
CL	MS 1137.5+6625	0.784	1.3033	0.2629
SN	03D4fd	0.791	0.6880	0.0665
RG	3C41	0.794	0.6315	0.0714
SN	03D1fq	0.800	0.7403	0.0920
RG	3C 265	0.811	0.5901	0.0793
CL	RX J1716.4+6708	0.813	0.4833	0.2184
RG	3C114	0.815	0.6368	0.0695
SN	04D3nc	0.817	0.6688	0.0647
SN	03D4cn	0.818	0.8111	0.1009
SN	04D3lu	0.822	0.6795	0.0688
CL	MS 1054.5-0321	0.826	0.6225	0.1264
RG	3C54	0.827	0.7573	0.0835
SN	04D3cp	0.830	0.6342	0.0496
SN	HST05Spo	0.839	0.5729	0.0554
SN	04D4bk	0.840	0.7110	0.0557
SN	sn2003eq	0.840	0.6336	0.0642
RG	3C6.1	0.840	0.7402	0.0861



Table 1—Continued

Type	Source	$z$	$y$	$\sigma_y$
SN	HST04Man	0.854	0.7187	0.0993
RG	3C 325	0.860	0.7080	0.1292
SN	03D1ew	0.868	0.7233	0.0566
CL	CL J1226.9+3332	0.890	0.5232	0.1696
SN	sn2003eb	0.900	0.6052	0.0725
SN	03D4di	0.905	0.6742	0.0497
SN	04D3gx	0.910	0.7973	0.0661
SN	04D3ki	0.930	0.8732	0.0764
SN	sn2003XX	0.935	0.6918	0.0956
SN	03D4cx	0.949	0.7996	0.0626
SN	04D3ml	0.950	0.7562	0.0522
SN	sn2002dd	0.950	0.6897	0.1112
SN	sn2003es	0.954	0.7975	0.1028
SN	HST04Tha	0.954	0.6482	0.0836
RG	3C 289	0.967	0.5950	0.1097
SN	HST04Pat	0.970	0.9380	0.1598
RG	3C 268.1	0.974	0.7458	0.1432
SN	HST04Omb	0.975	0.7570	0.0941
RG	3C 280	0.996	0.6477	0.1221
SN	04D3dd	1.010	0.9494	0.0743
SN	HST05Str	1.010	0.9627	0.0887
SN	HST05Fer	1.020	0.6688	0.0862
SN	HST04Eag	1.020	0.8537	0.0786
RG	3C 356	1.079	0.8735	0.1842
SN	HST05Gab	1.120	0.8716	0.0763
SN	sn2002ki	1.140	0.8795	0.1215
SN	HST04Gre	1.140	0.7767	0.1145
RG	3C 267	1.144	0.7136	0.1396
RG	3C 194	1.190	1.0074	0.2047
RG	3C 324	1.210	1.0208	0.3089
SN	HST05Koe	1.230	1.0432	0.1153

Table 1—Continued

Type	Source	$z$	$y$	$\sigma_y$
SN	HST05Lan	1.230	0.9514	0.0920
SN	sn2002fw	1.300	0.9615	0.0930
SN	sn2002hp	1.305	0.7447	0.1063
RG	3C469.1	1.336	1.1364	0.3255
SN	sn2003dy	1.340	0.8860	0.1306
SN	HST04Mcg	1.370	1.0091	0.1208
SN	HST04Sas	1.390	0.8595	0.0792
RG	3C 437	1.480	0.9299	0.2697
RG	3C 68.2	1.575	1.5748	0.4873
RG	3C 322	1.681	1.3078	0.3400
SN	sn1977ff	1.755	0.9174	0.1521
RG	3C 239	1.790	1.3666	0.3382

Table 2. Fits in Independent Redshift Bins to 192 Supernovae and 30 Radio Galaxies

Bin	N	$z_{med}$	$z_{min}$	$z_{max}$	$y'(z_{med})$	$H(z_{med})/H_0$	$y''(z_{med})$	$q(z_{med})$
1/6	37	0.025	0.016	0.052	$1.09 \pm 0.05$	$0.92 \pm 0.05$	$-6.2 \pm 7.5$	$4.8 \pm 6.9$
2/6	37	0.275	0.054	0.348	$0.74 \pm 0.07$	$1.34 \pm 0.13$	$-1.6 \pm 0.8$	$1.9 \pm 1.6$
3/6	37	0.430	0.352	0.504	$0.67 \pm 0.15$	$1.48 \pm 0.32$	$2.7 \pm 6.50$	—
4/6	37	0.600	0.508	0.670	$0.72 \pm 0.28$	$1.4 \pm 0.5$	$1.2 \pm 11$	—
5/6	37	0.790	0.679	0.905	$0.55 \pm 0.16$	$1.8 \pm 0.5$	$-4.0 \pm 5.0$	—
6/6	37	1.100	0.910	1.790	$0.40 \pm 0.13$	$2.5 \pm 0.8$	$-0.4 \pm 0.8$	$1.1 \pm 3.7$
1/4	55	0.035	0.016	0.268	$1.03 \pm 0.03$	$0.97 \pm 0.03$	$-0.9 \pm 0.6$	$-0.1 \pm 0.6$
2/4	55	0.400	0.274	0.502	$0.79 \pm 0.08$	$1.27 \pm 0.13$	$-0.4 \pm 2.5$	$-0.2 \pm 4.5$
3/4	55	0.630	0.504	0.749	$0.54 \pm 0.12$	$1.85 \pm 0.40$	$-2.50 \pm 3.2$	—
4/4	57	0.965	0.752	1.790	$0.64 \pm 0.10$	$1.57 \pm 0.23$	$-0.9 \pm 0.5$	$1.80 \pm 1.3$
1/3	74	0.050	0.016	0.348	$1.02 \pm 0.03$	$0.98 \pm 0.03$	$-1.05 \pm 0.27$	$0.08 \pm 0.26$
2/3	74	0.505	0.352	0.670	$0.80 \pm 0.06$	$1.26 \pm 0.09$	$0.9 \pm 1.4$	$-2.7 \pm 2.6$
3/3	74	0.905	0.679	1.790	$0.66 \pm 0.06$	$1.52 \pm 0.15$	$-0.8 \pm 0.3$	$1.2 \pm 0.9$
1/2	111	0.275	0.016	0.504	$0.84 \pm 0.02$	$1.19 \pm 0.03$	$-0.73 \pm 0.16$	$0.10 \pm 0.27$
2/2	111	0.790	0.508	1.790	$0.63 \pm 0.04$	$1.59 \pm 0.10$	$-0.40 \pm 0.21$	$0.13 \pm 0.57$

Table 3. Fits in Independent Redshift Bins at the Median Redshift of the Bin

Data	$P_{DE}/\rho_{0c}$	$\rho_{DE}/\rho_{0c}$	$w_{DE}$	$V_{DE}/\rho_{0c}$	$K_{DE}/\rho_{0c}$	$s$
1/2	$-0.38 \pm 0.24$	$0.79 \pm 0.07$	$-0.48 \pm 0.34$	$0.58 \pm 0.10$	$0.21 \pm 0.15$	$-0.75 \pm 0.21$
2/2	$-0.6 \pm 1.0$	$0.8 \pm 0.3$	$-0.8 \pm 1.2$	$0.7 \pm 0.6$	$0.1 \pm 0.45$	$-0.50 \pm 0.25$

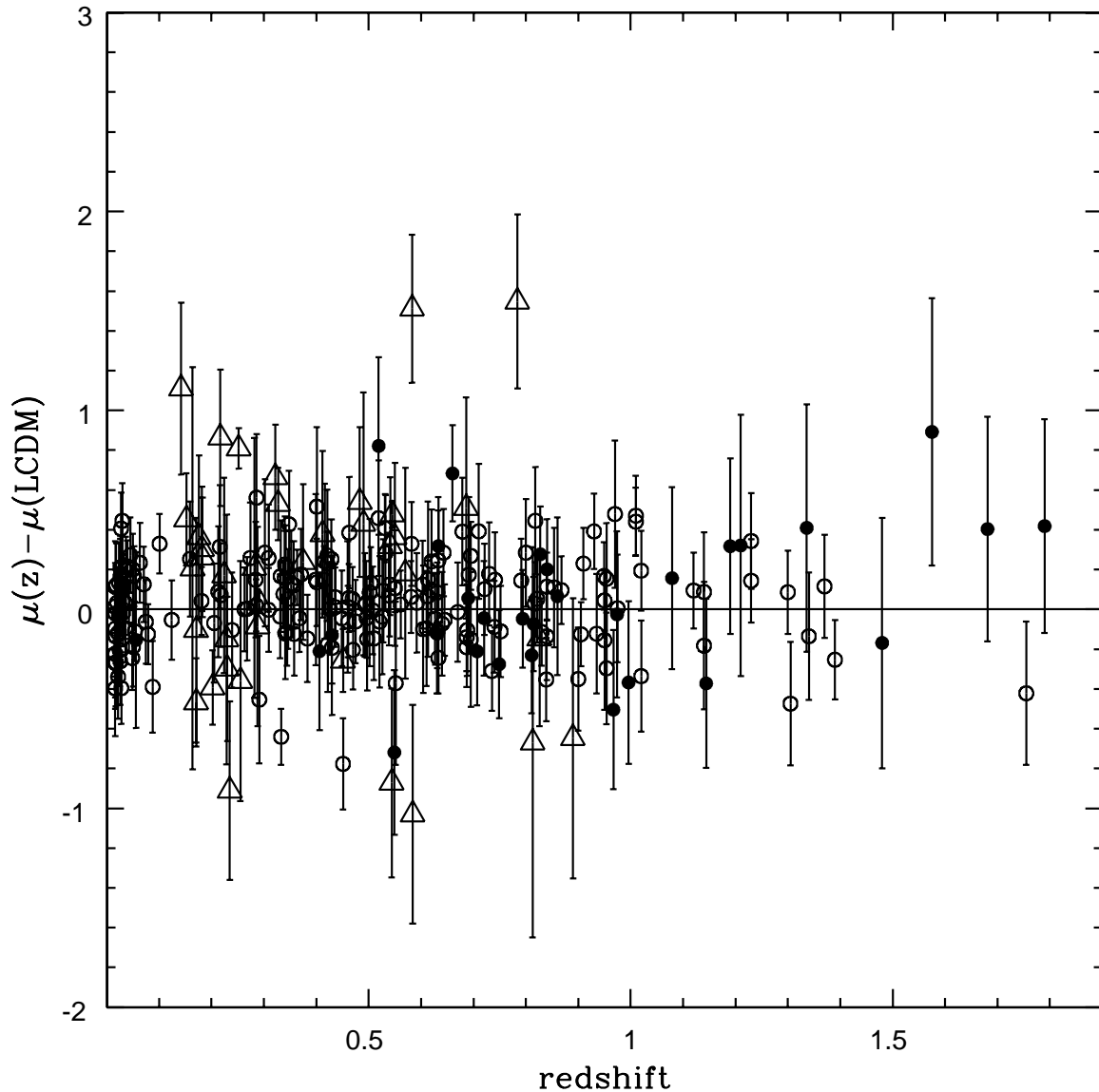


Fig. 1.— The difference between the distance modulus to the source and that expected in a standard LCDM model with  $\Omega_m = 0.3$  and  $\Omega_\Lambda = 0.7$ . Open circles represent the 192 supernovae of Davis et al. (2007), filled circles represent the 30 radio galaxies of Daly et al. (2007), and open triangles represent the 38 clusters of Bonamente et al. (2006).

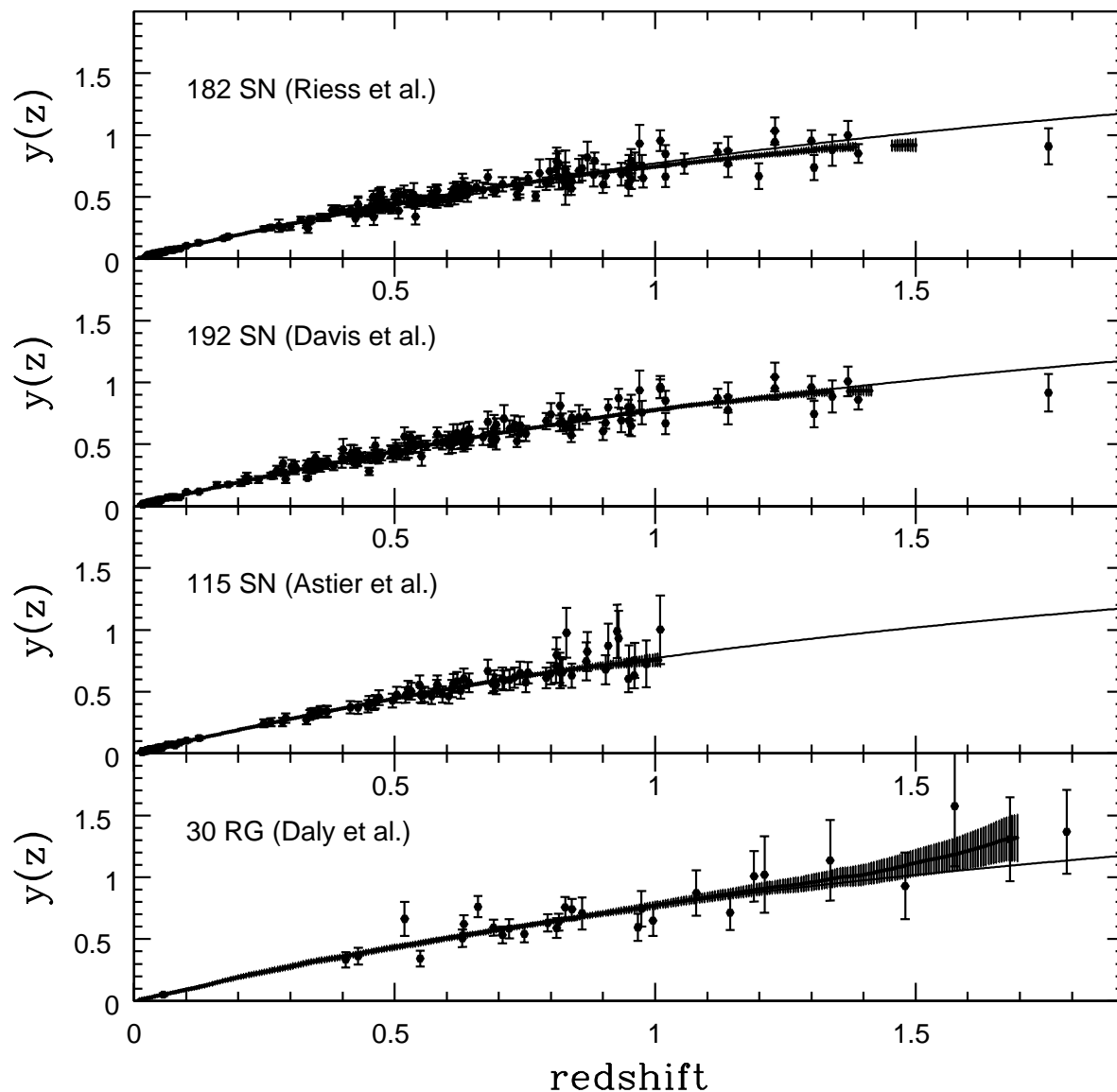


Fig. 2.— The dimensionless coordinate distances to each source show along with the best fit  $y(z)$  and its one sigma error bar for the 182 gold supernovae from Riess et al. (2007), the 192 supernovae from Davis et al. (2007), the 115 supernovae of Astier et al. (2006), and the 30 radio galaxies from Daly et al. (2007). In this and in all subsequent figures, the solid curve illustrates the predicted value in a standard LCDM model with  $\Omega_m = 0.3$  and  $\Omega_\Lambda = 0.7$ .

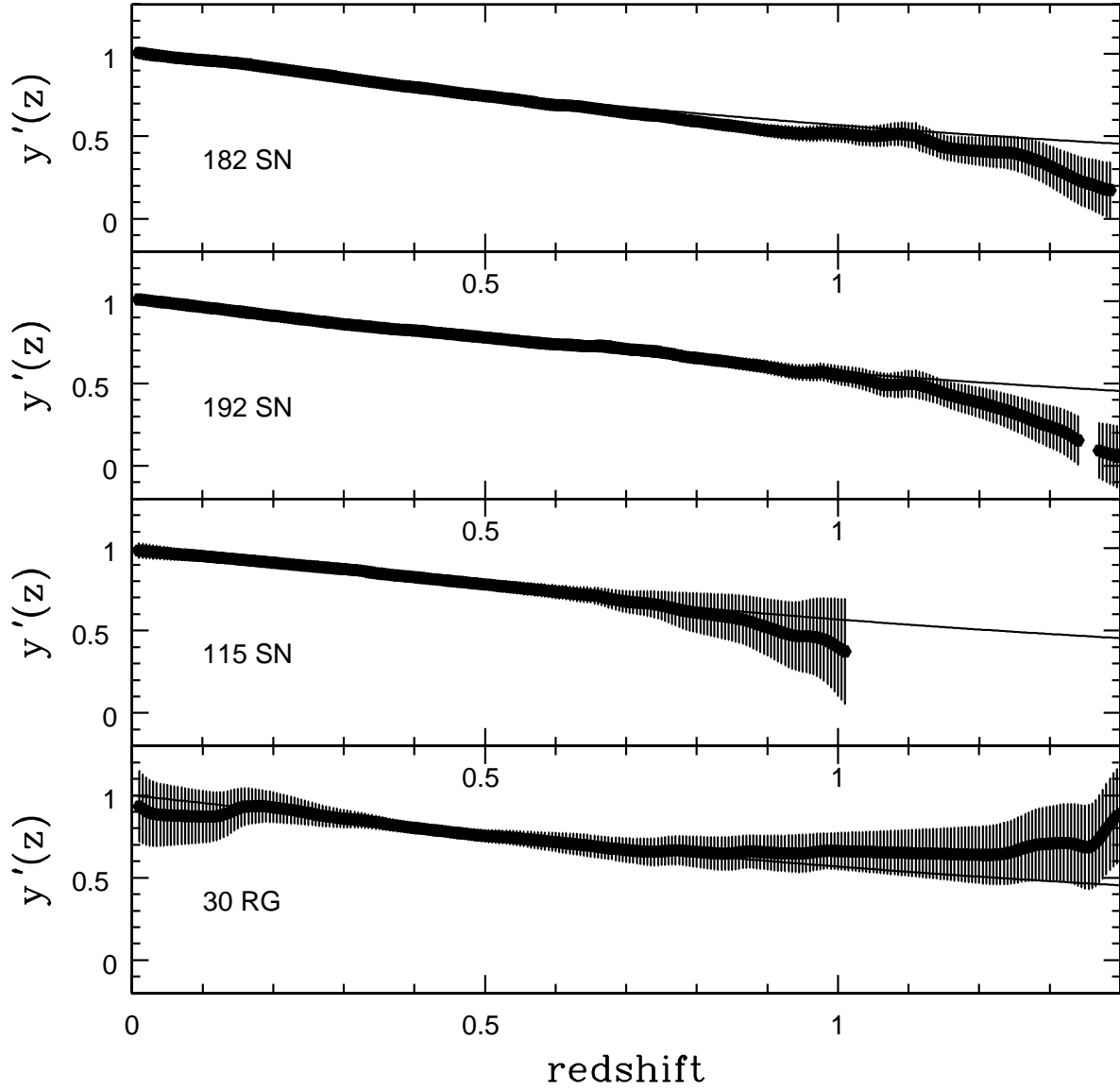


Fig. 3.— The first derivative of the coordinate distance with respect to redshift as a function of redshift for the samples described in Fig. 2.

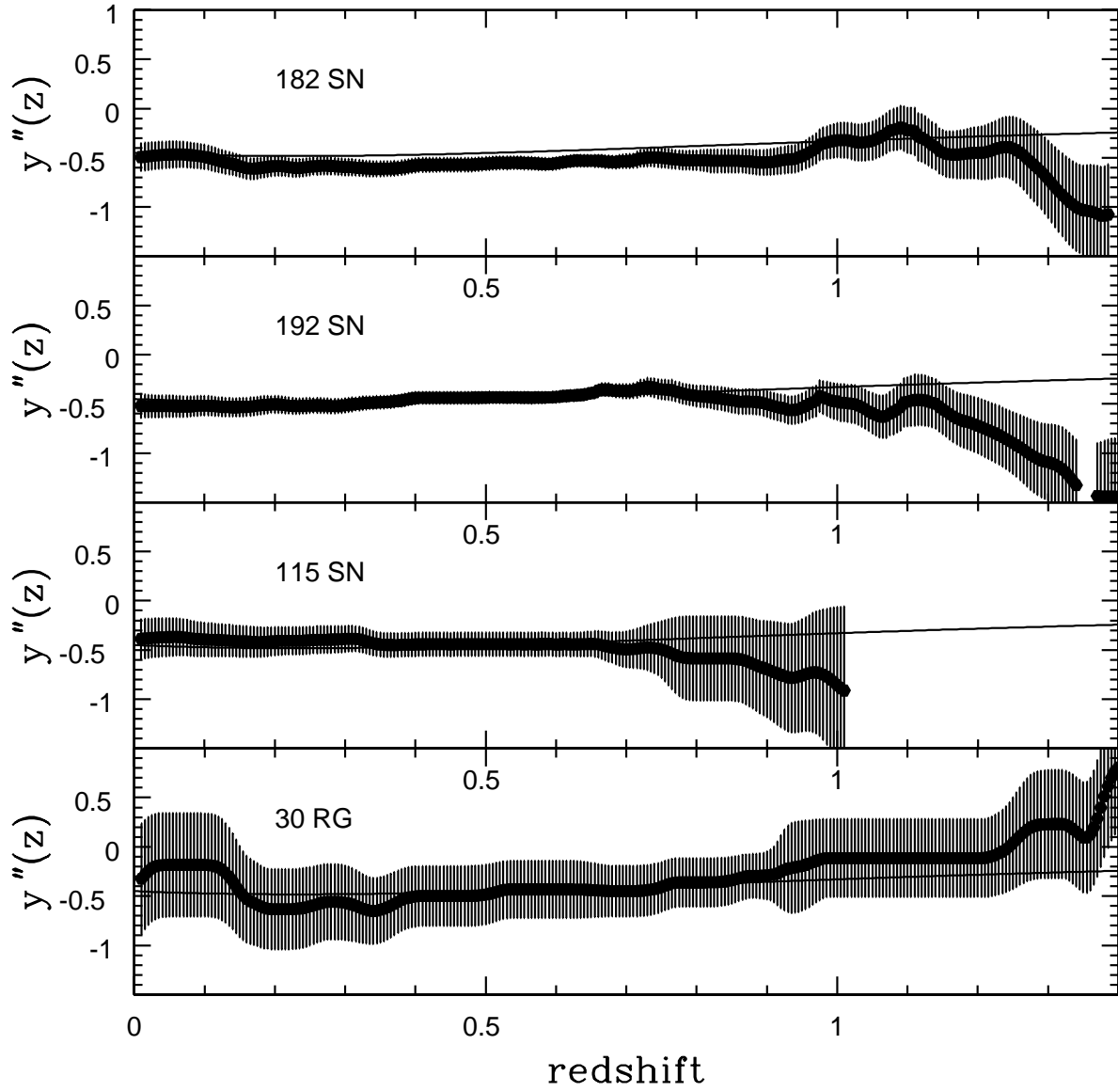


Fig. 4.— The second derivative of the coordinate distance with respect to redshift as a function of redshift for the samples described in Fig. 2.

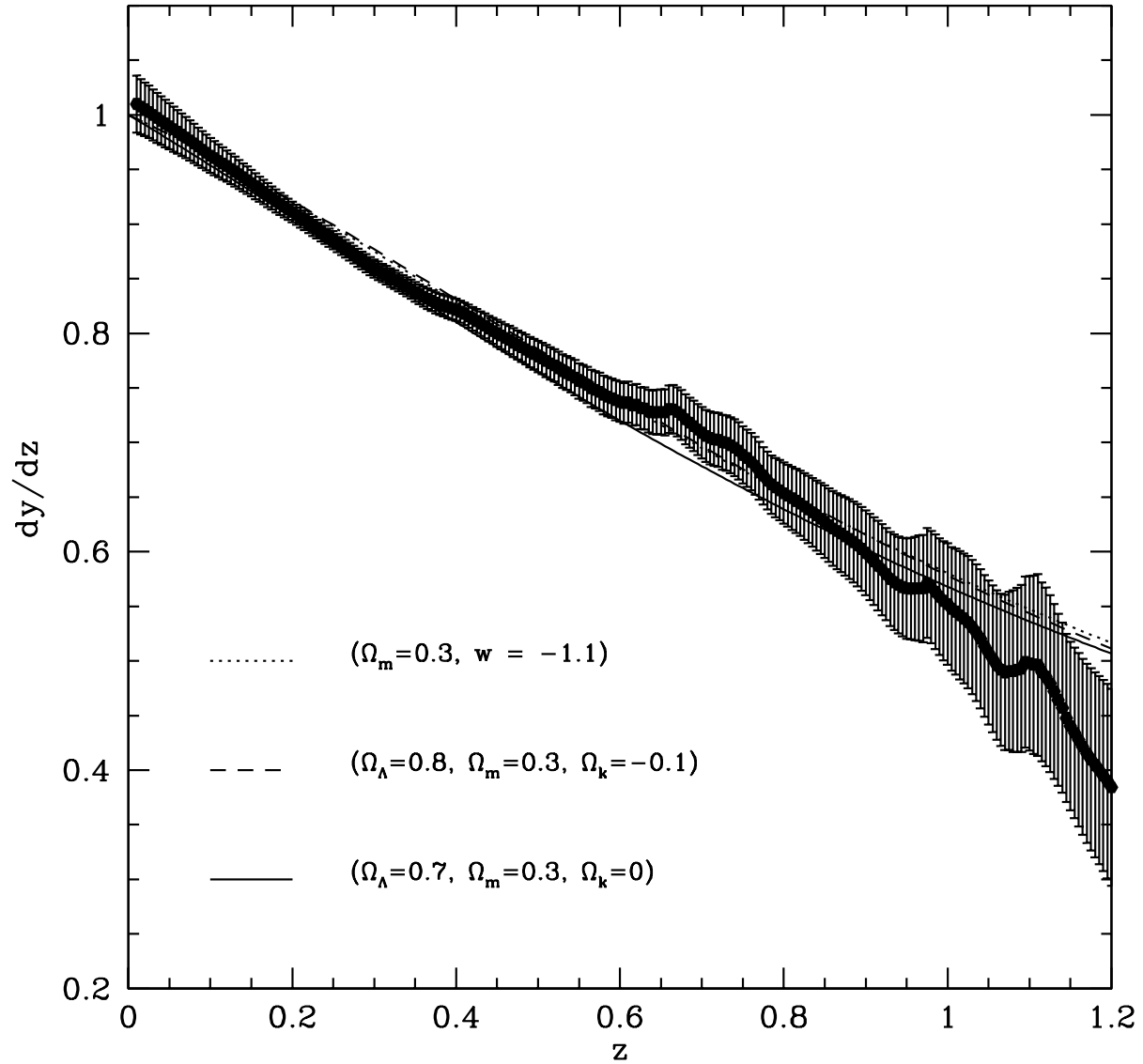


Fig. 5.— The first derivative of the coordinate distance with respect to redshift as a function of redshift for the Davis et al. (2007) sample of 192 supernovae. Lines illustrating the predicted values of  $y'(z)$  for the best fit parameters obtained fitting to a spatially flat quintessence model and a lambda model with space curvature, as well as a standard flat LCDM model, are shown.



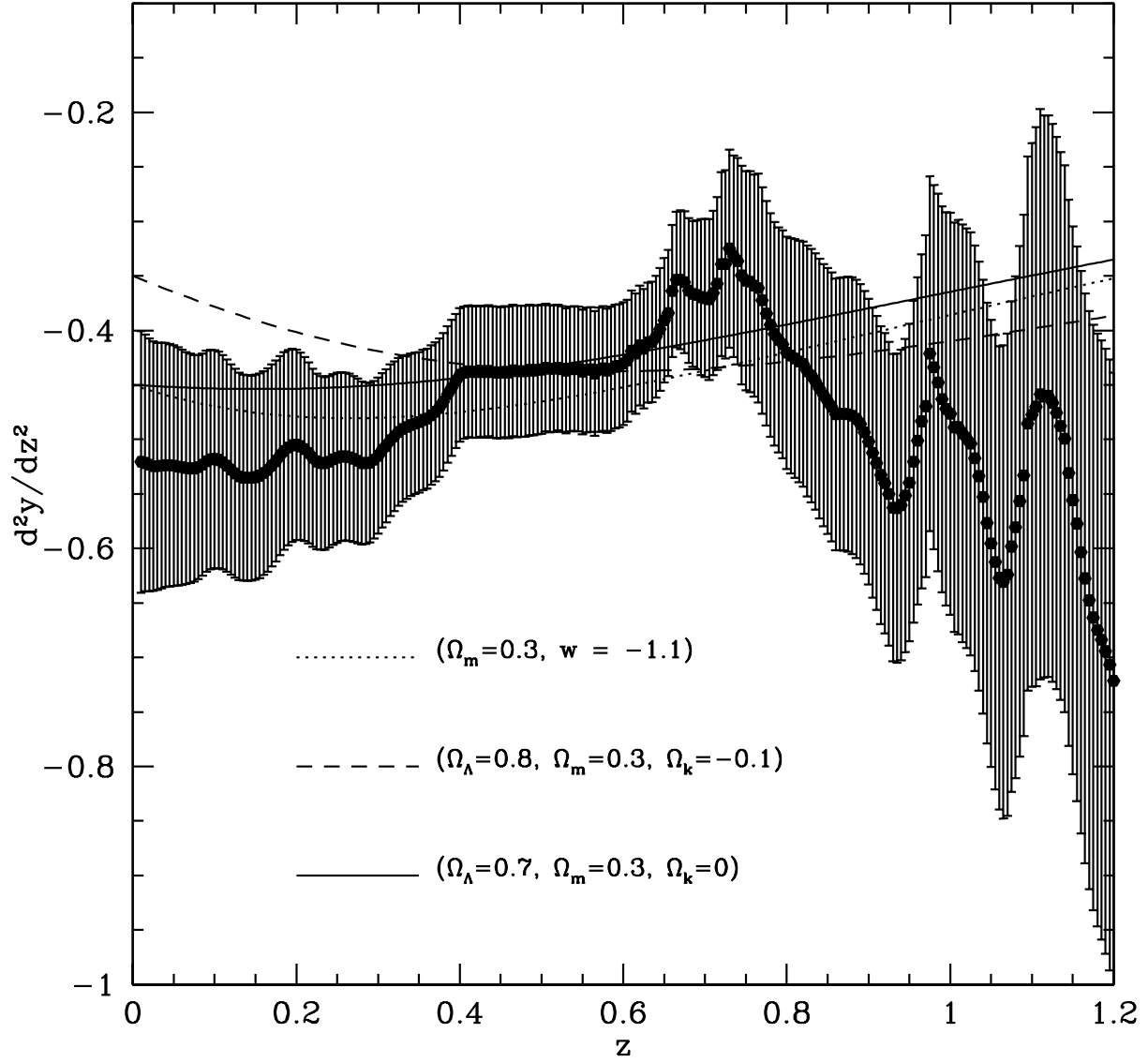


Fig. 6.— As in Figure 5 for the second derivative of the coordinate distance with respect to redshift.

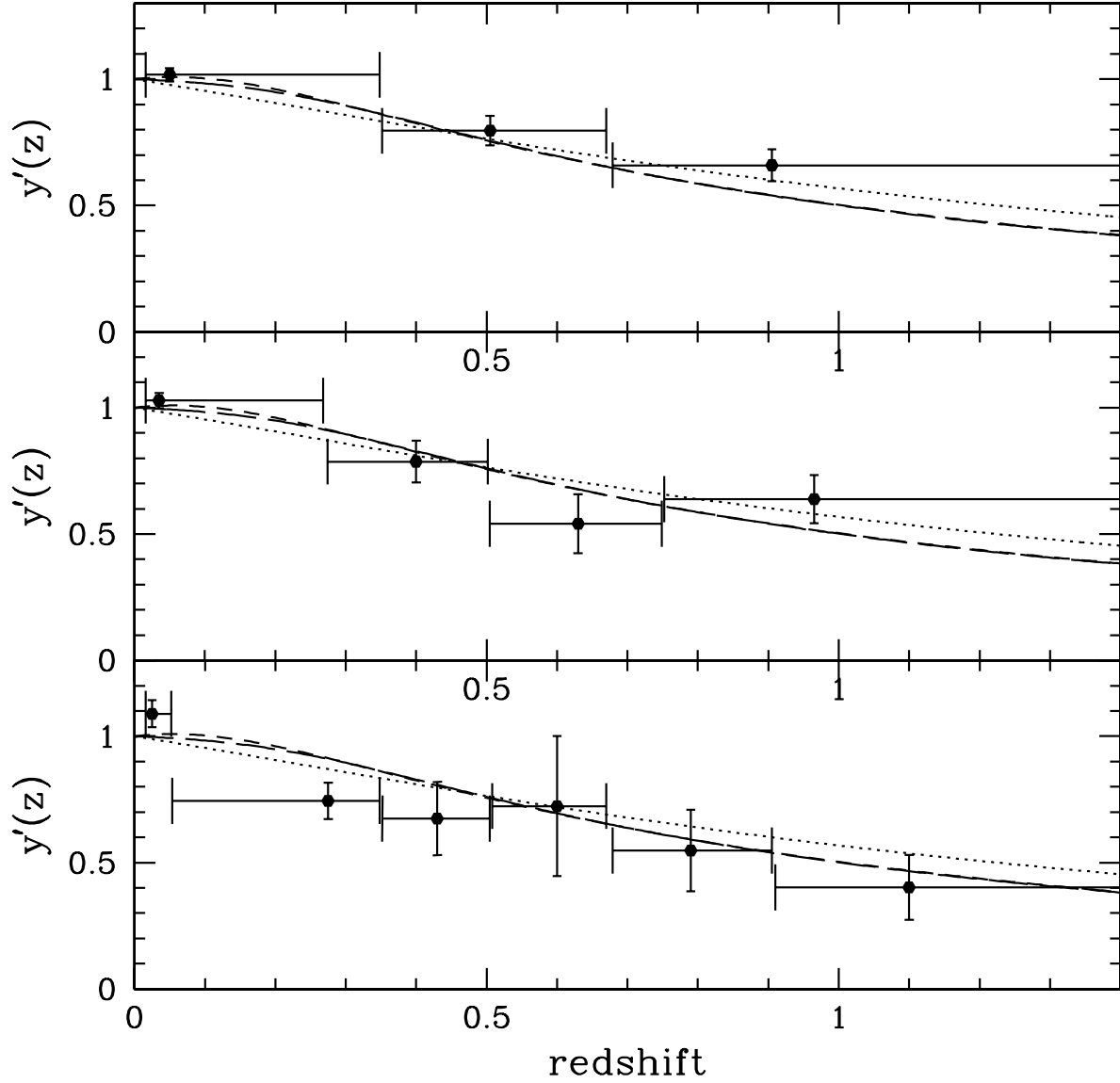


Fig. 7.— Results obtained for the first derivative of the coordinate distance with respect to redshift for the combined sample of 192 supernovae and 30 radio galaxies using data split into three bins (top panel), four bins (middle panel), and six bins (bottom panel). The data point at the median redshift is shown, and the horizontal bars indicate the redshift range of the data points in the bin. The standard LCDM prediction for  $\Omega_m = 0.3$  is indicated by the dotted line, and the curves predicted by the Cardassian model and the generalized Chaplygin gas model, which yield nearly identical results, are shown by the short and long dashed curves.

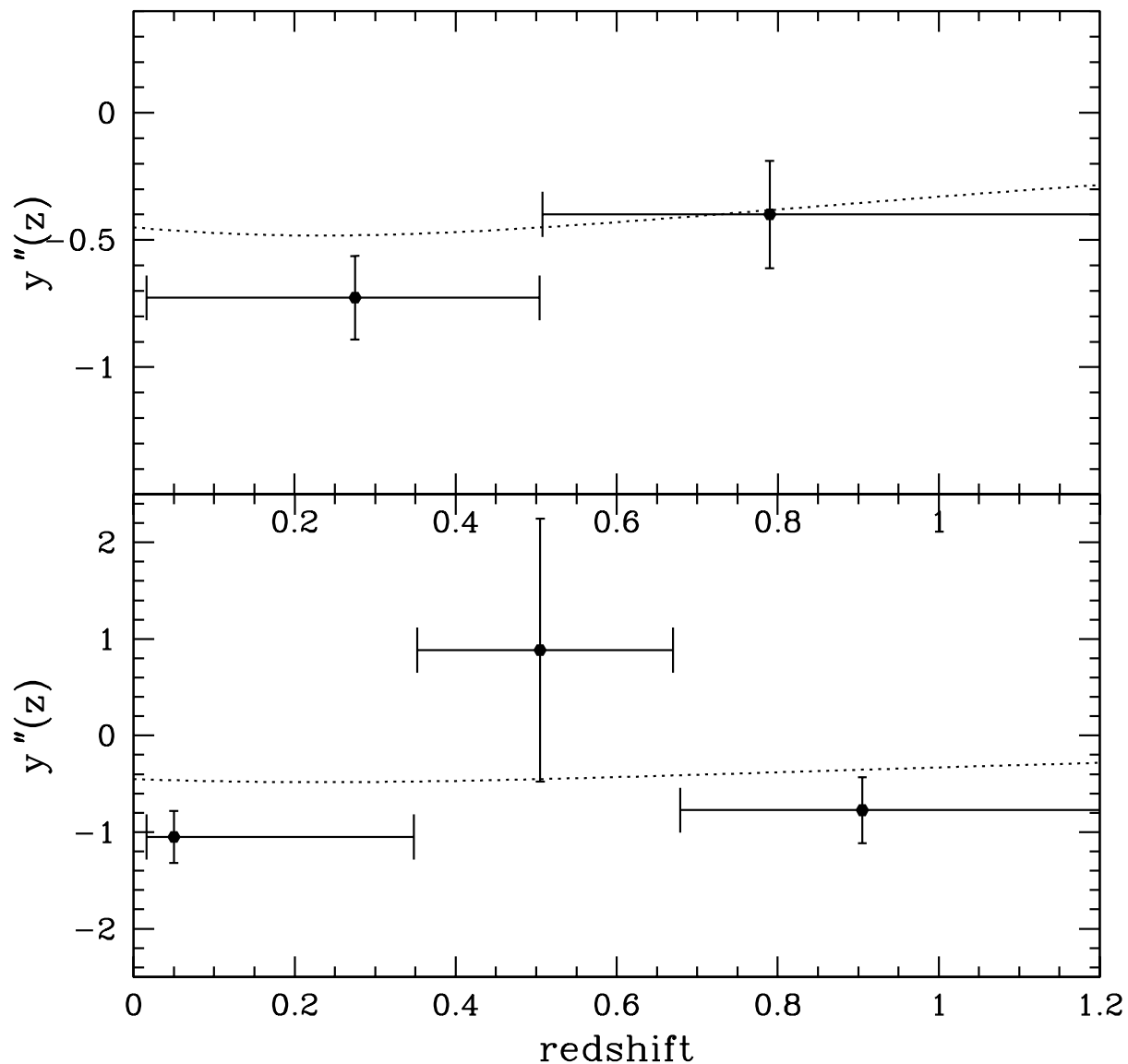


Fig. 8.— Results obtained for the second derivative of the coordinate distance with respect to redshift for the combined sample of 192 supernovae and 30 radio galaxies using data split into two bins (top panel) and three (bottom panel). The data point at the median redshift is shown, and the horizontal bars indicate the redshift range of the data points in the bin. The standard LCDM prediction for  $\Omega_m = 0.3$  is indicated by the dotted line.

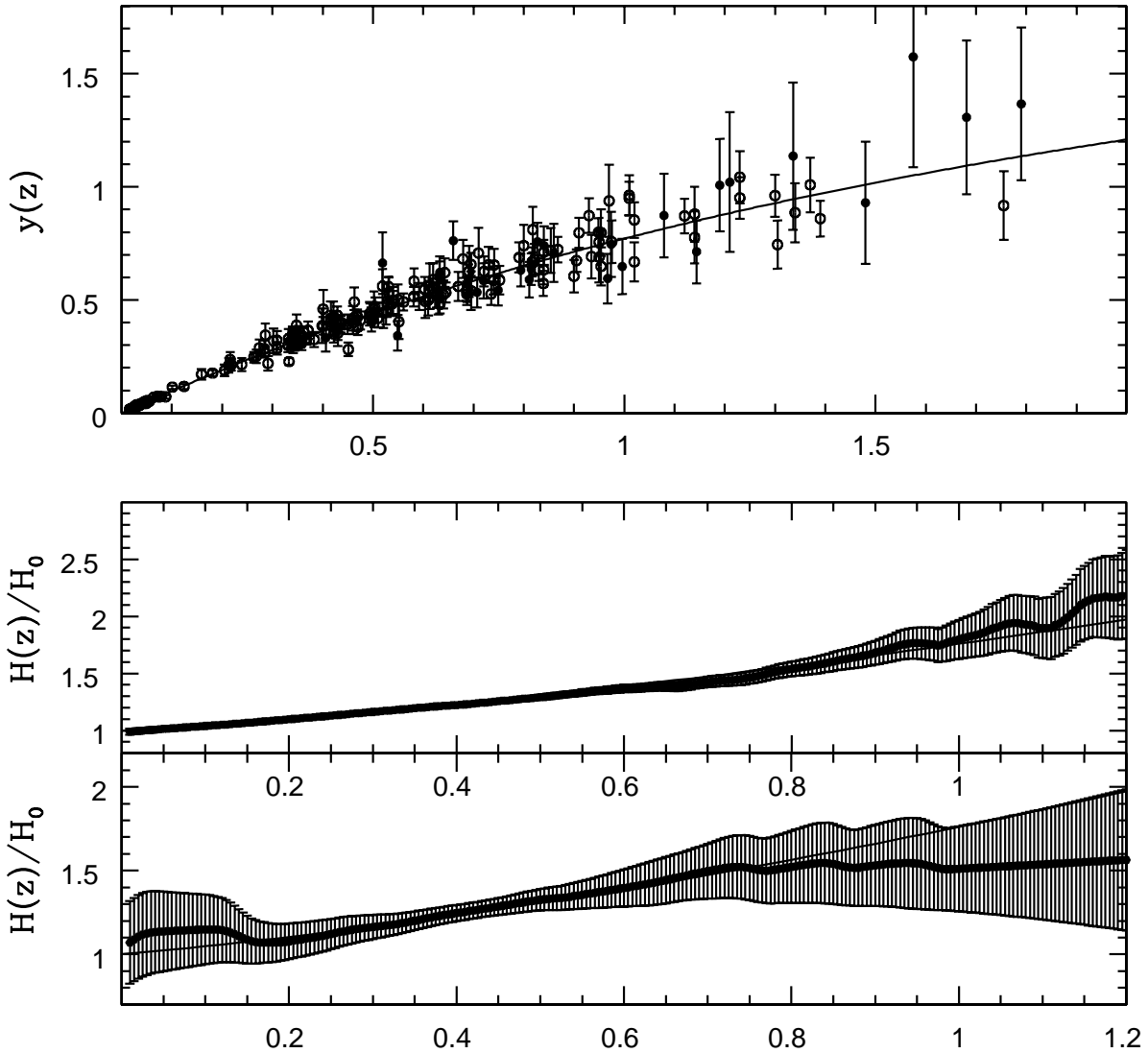


Fig. 9.— The dimensionless coordinate distances to the 192 supernovae of Davis et al. (2007) (open circles) and the 30 radio galaxies of Daly et al. (2007) (closed circles) are shown in the top panel. Our model-independent determination of  $H(z)$ , obtained assuming only a FRW metric and zero space curvature, is shown for the combined sample of 192 supernovae and 30 radio galaxies in the second panel, while that for the 30 radio galaxies alone is shown in the bottom panel.

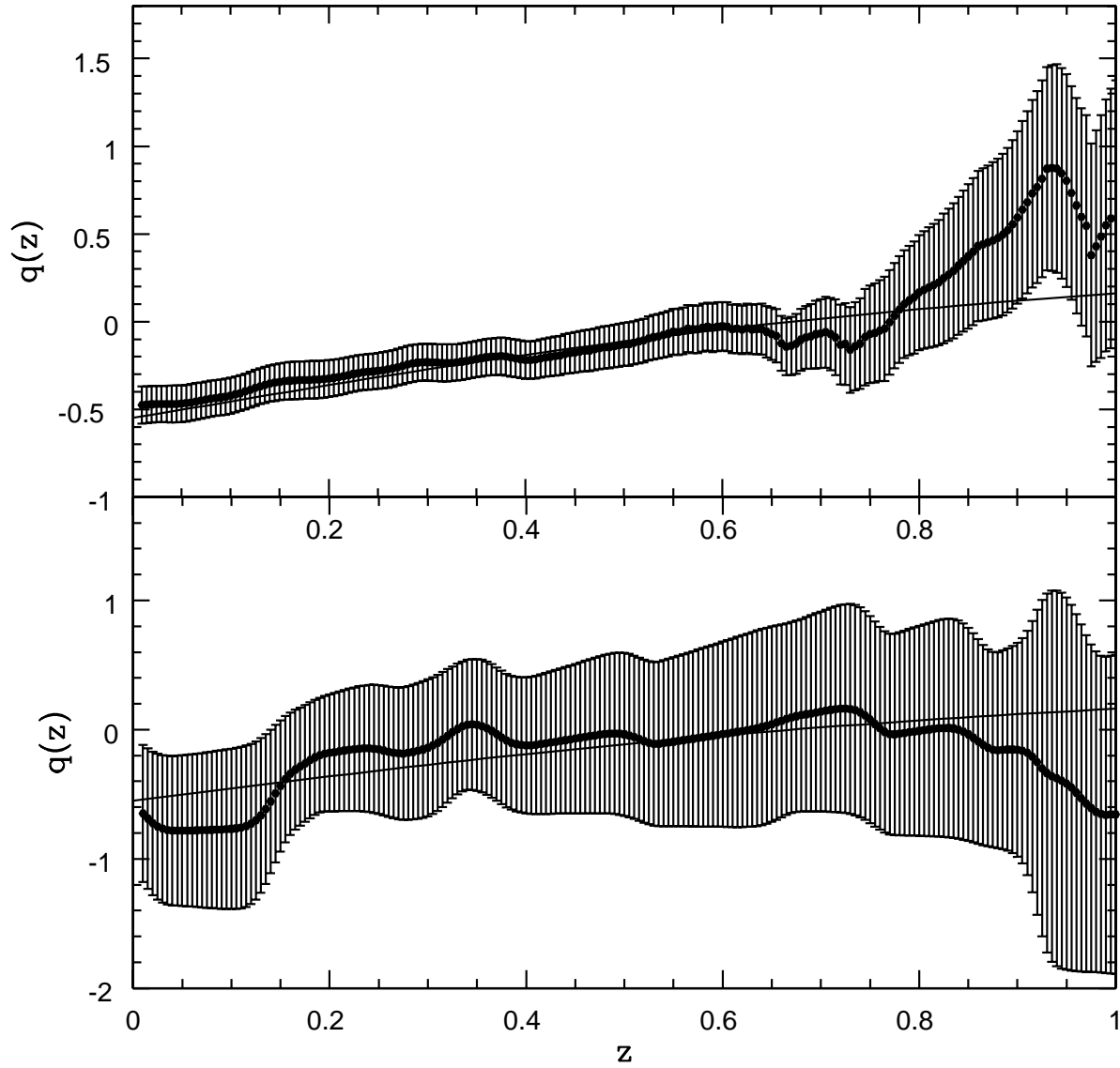


Fig. 10.— Our model-independent determination of  $q(z)$ , obtained assuming only a FRW metric and zero space curvature, is shown for the combined sample of 192 supernovae and 30 radio galaxies in the top panel and for the 30 radio galaxies alone in the bottom panel.

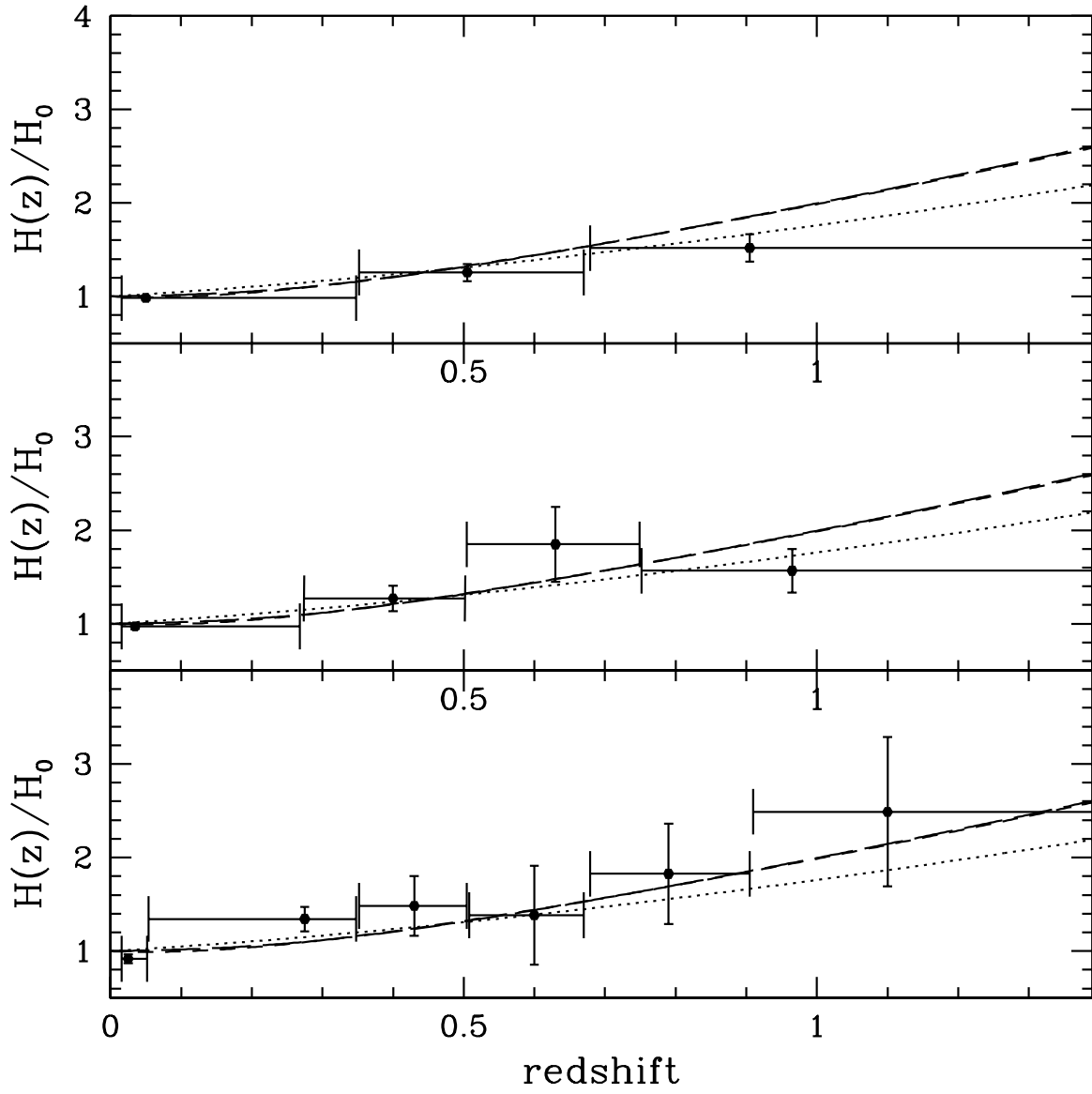


Fig. 11.— As in Figure 7 but for  $H(z_{med})/H_0$ .

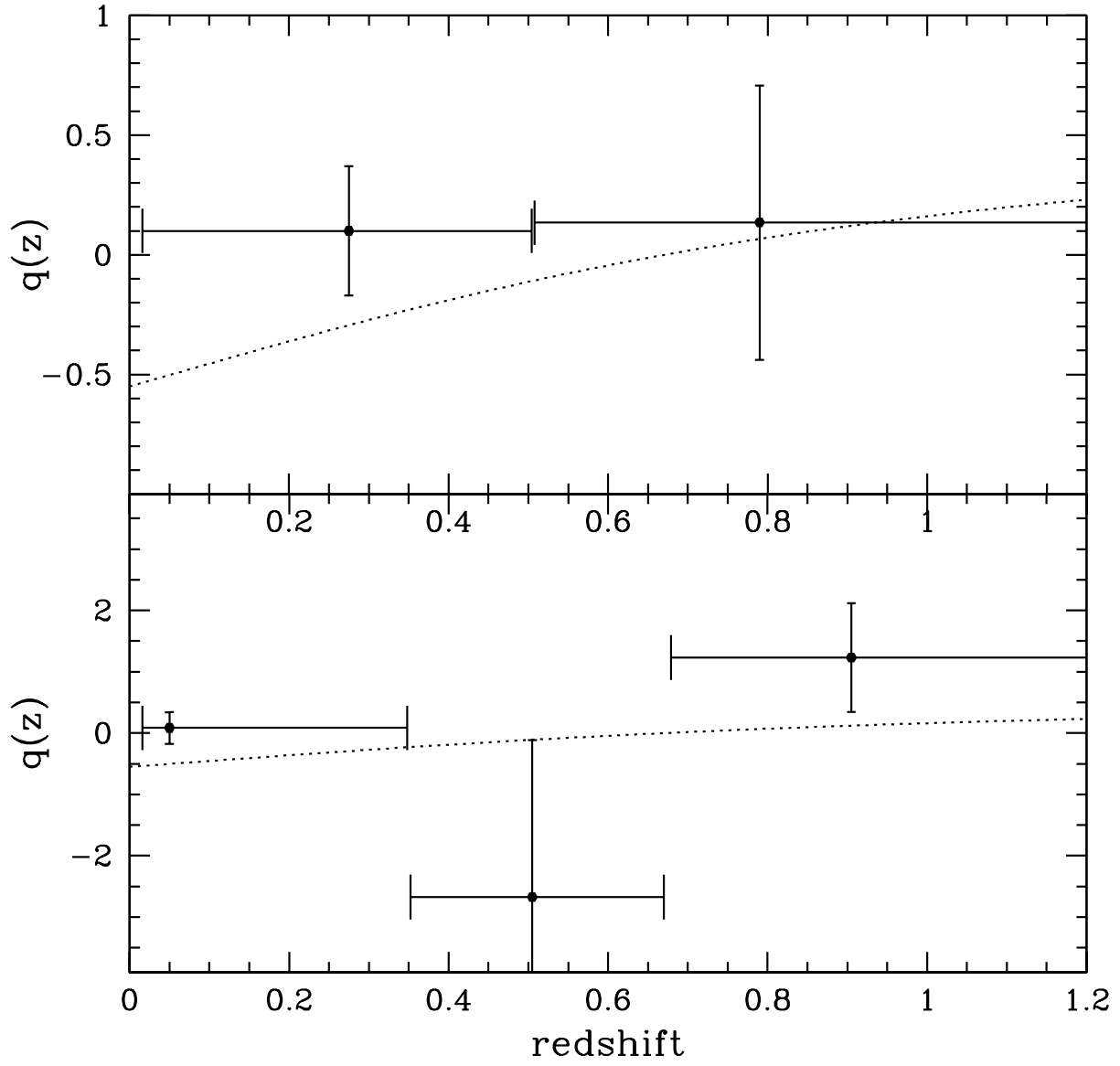


Fig. 12.— As in Figure 8 but for  $q(z_{med})$ .

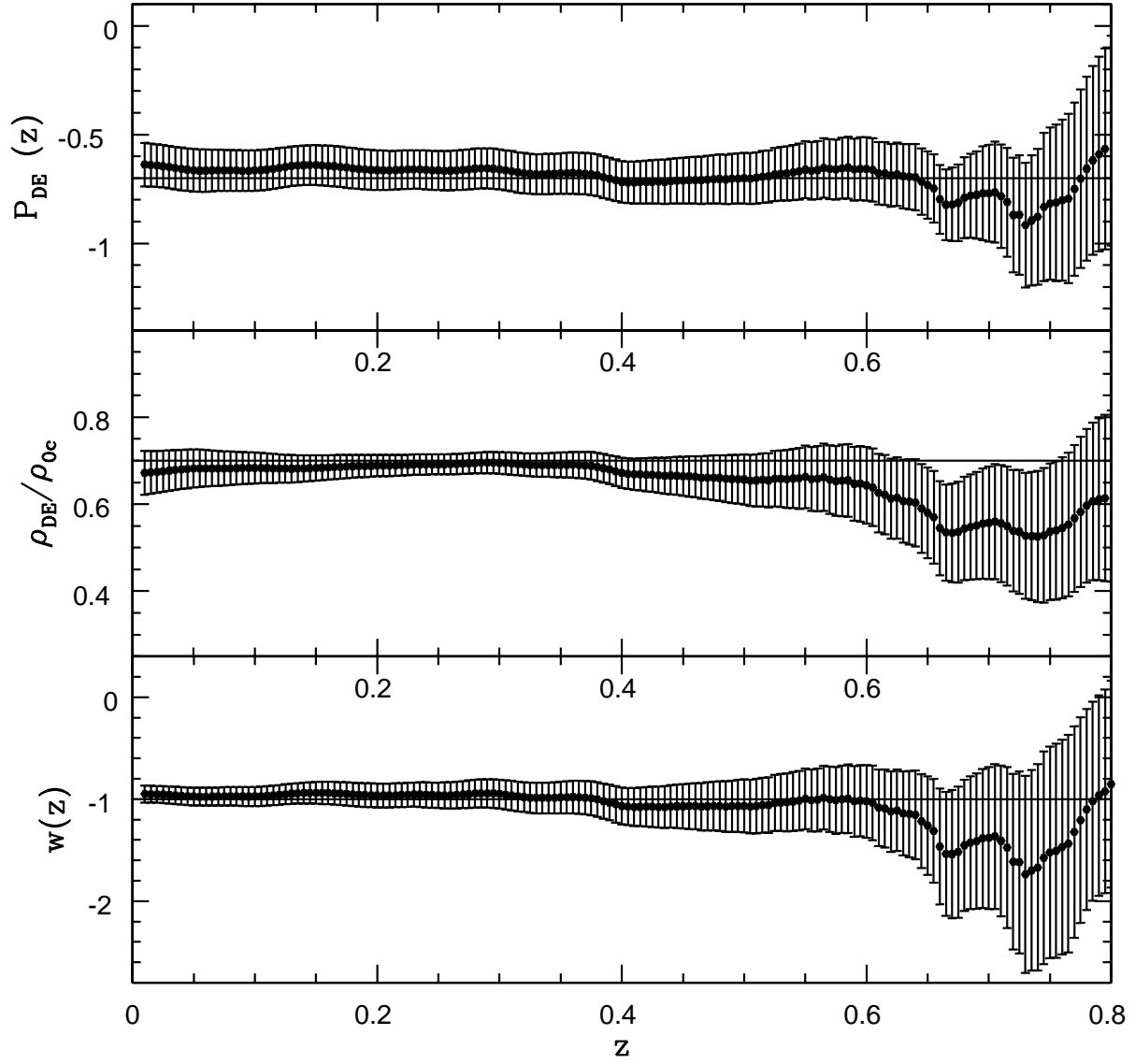


Fig. 13.— The pressure, energy density, and equation of state of the dark energy obtained for the combined sample of 30 radio galaxies and 192 supernovae, obtained from  $y'$  and  $y''$  assuming zero space curvature.



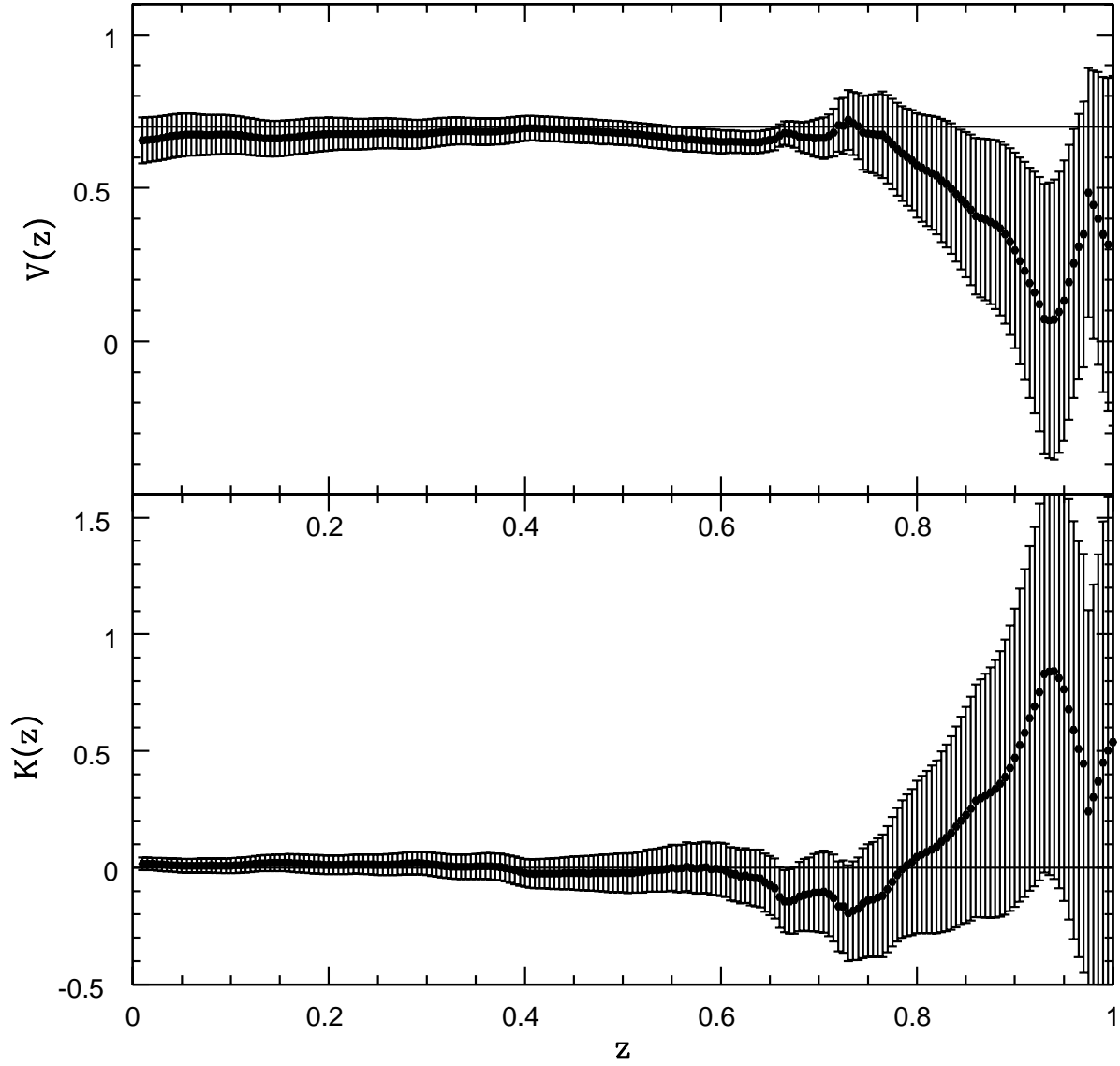


Fig. 14.— The potential and kinetic energy density of a dark energy scalar field as a function of redshift for the combined sample of 30 radio galaxies and 192 supernovae, obtained from  $y'$  and  $y''$  assuming zero space curvature.

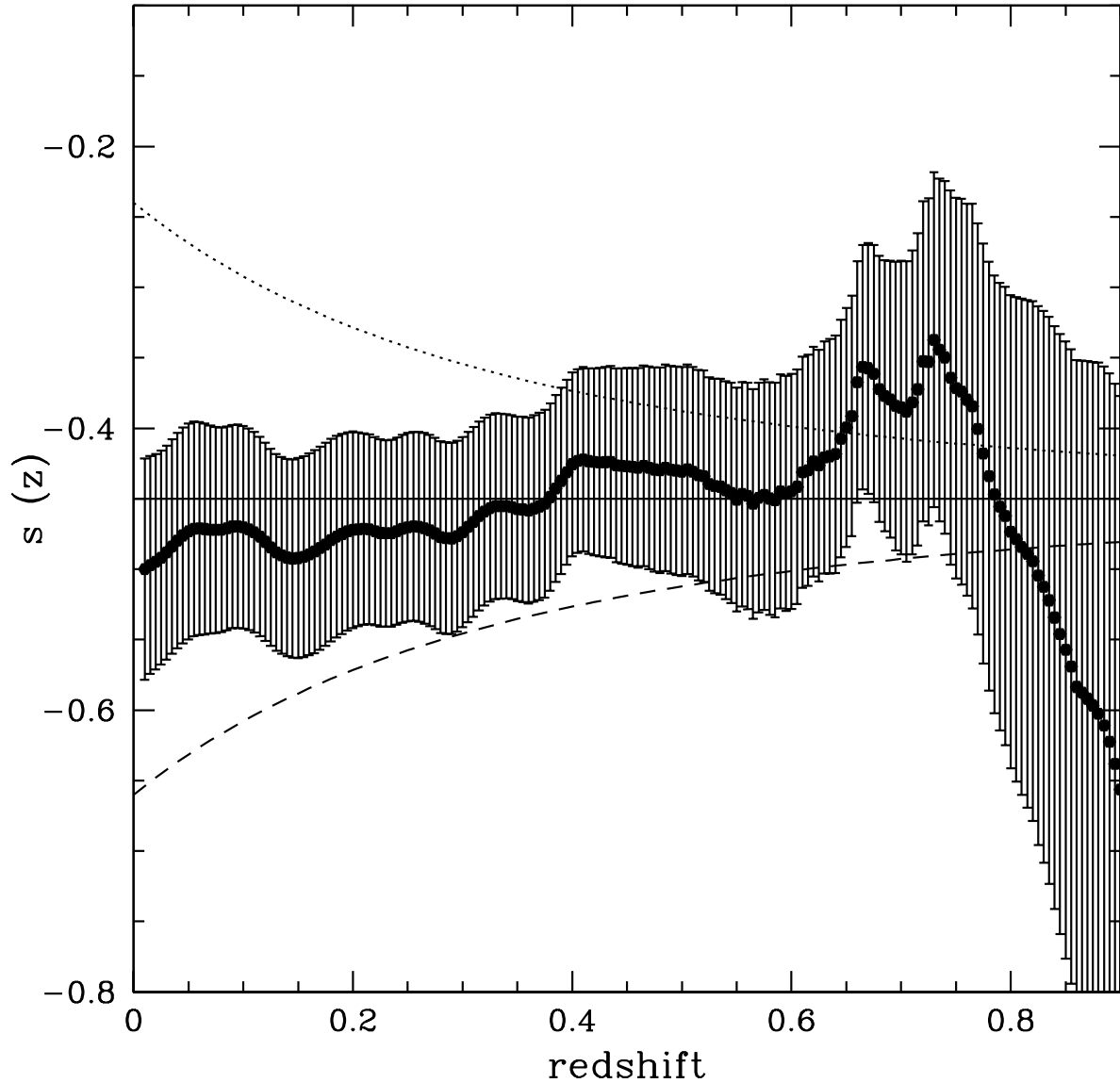


Fig. 15.— The dark energy indicator for the combined sample of 30 radio galaxies and 192 supernovae obtained from using equation 10. The behavior of  $s$  predicted using equation 11 is shown for three simple models each assuming  $\Omega_m = 0.3$ ,  $\Omega_{DE} = 0.7$  and  $f(z) = 1$  over the redshift range shown, and  $w = -1$  (solid line),  $w = -0.8$  and remains constant over the redshift range shown (long dashed curve), and  $w = -1.2$  and remains constant over the redshift range shown (short dashed curve). If  $s$  remains constant, it suggests that  $w = -1$ , and the value of  $s$  provides a new and independent measure of  $\Omega_m$ .

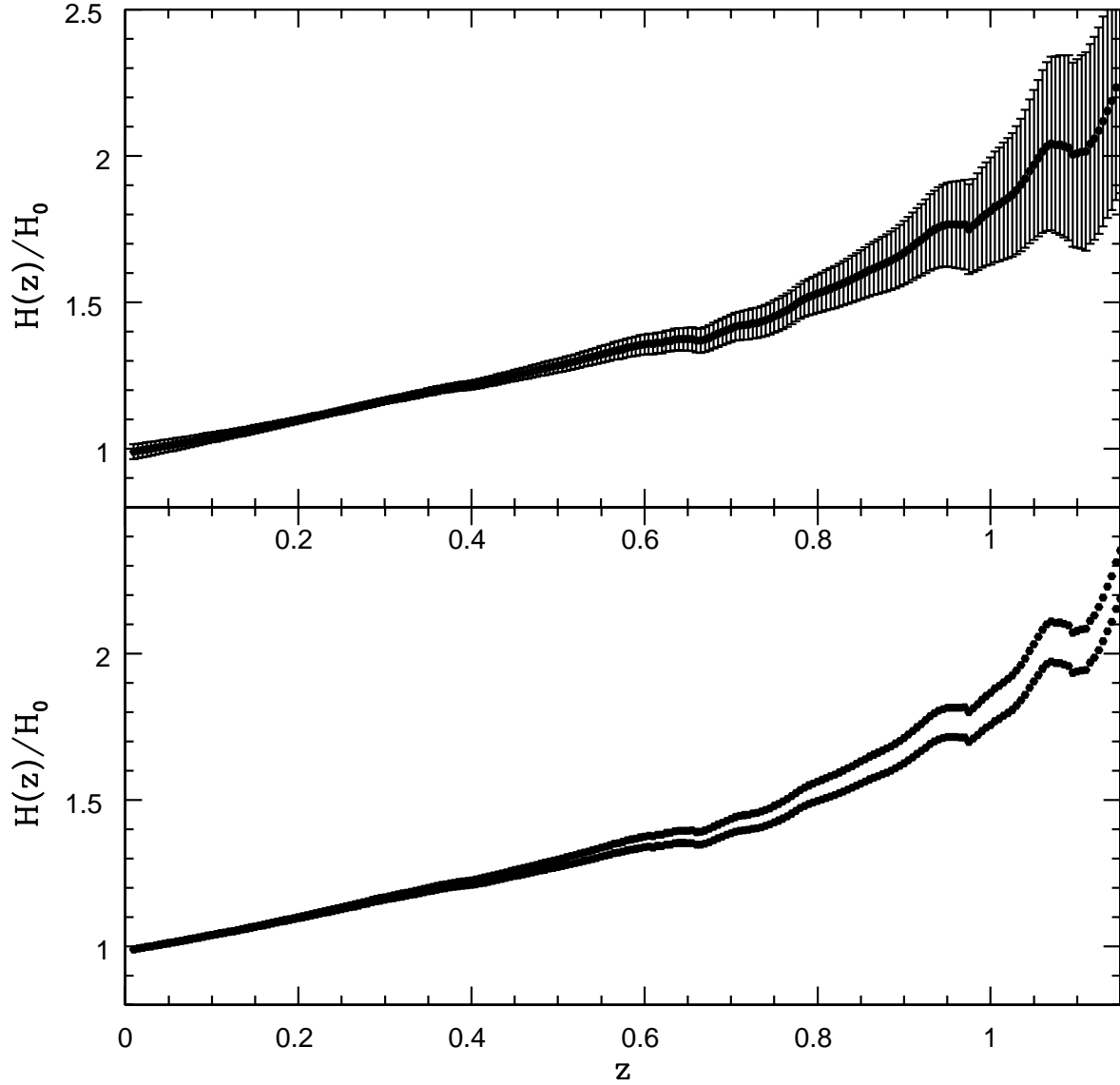


Fig. 16.— Model independent determination of  $H(z)$  for the Davis et al. (2007) sample of 192 supernovae. The top panel shows results obtained for  $\Omega_k = 0$ , and the bottom panel shows results obtained for  $\Omega_k = 0.1$  (upper curve) and  $\Omega_k = -0.1$  (lower curve). For clarity, the uncertainties are not shown on the bottom panel, but are similar to those shown on the top panel.

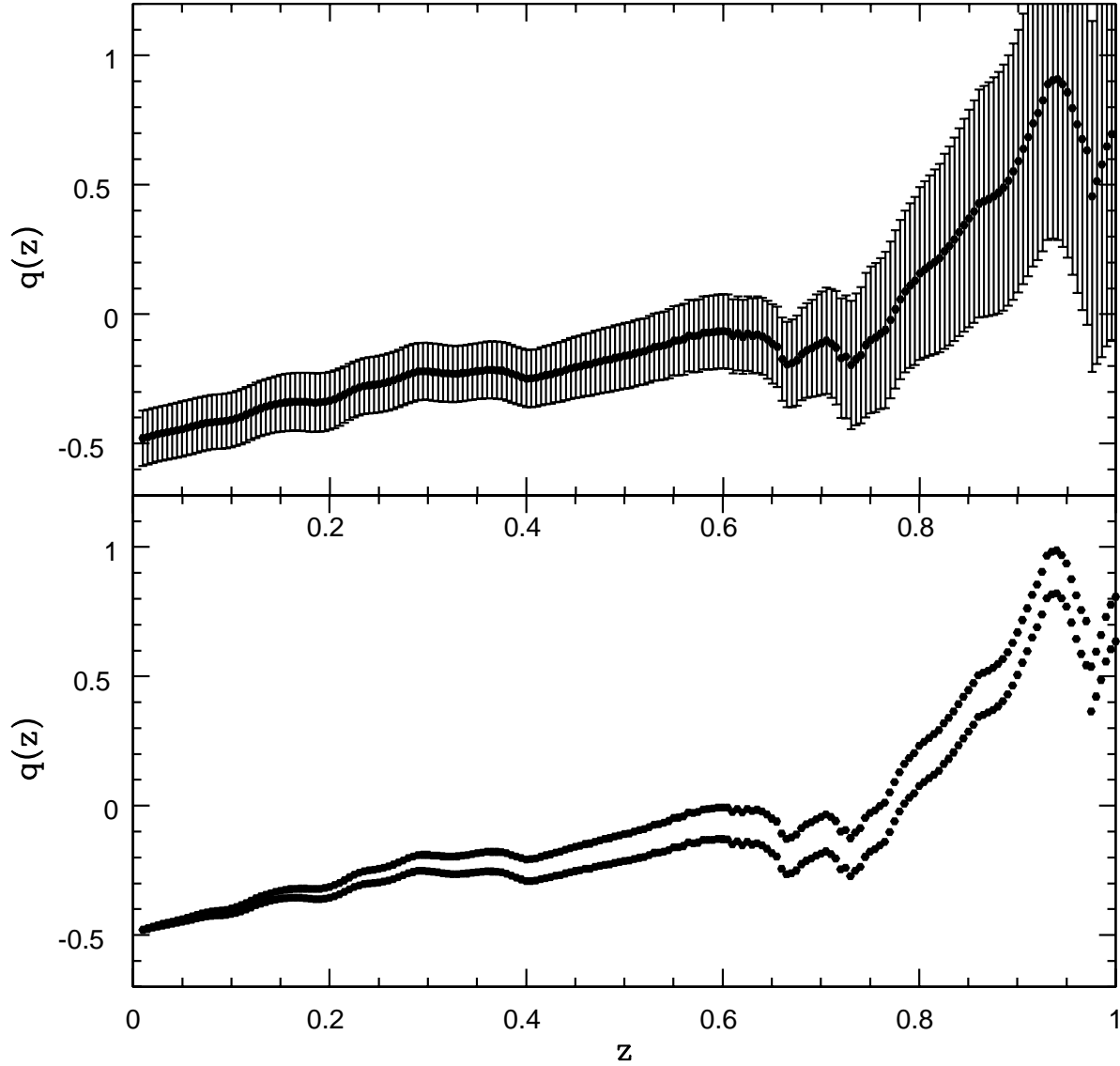


Fig. 17.— Model independent determination of  $q(z)$  for the Davis et al. (2007) sample of 192 supernovae. The top panel shows results obtained for  $\Omega_k = 0$ , and the bottom panel shows results obtained for  $\Omega_k = 0.1$  (upper curve) and  $\Omega_k = -0.1$  (lower curve). For clarity, the uncertainties are not shown on the bottom panel, but are similar to those shown on the top panel.

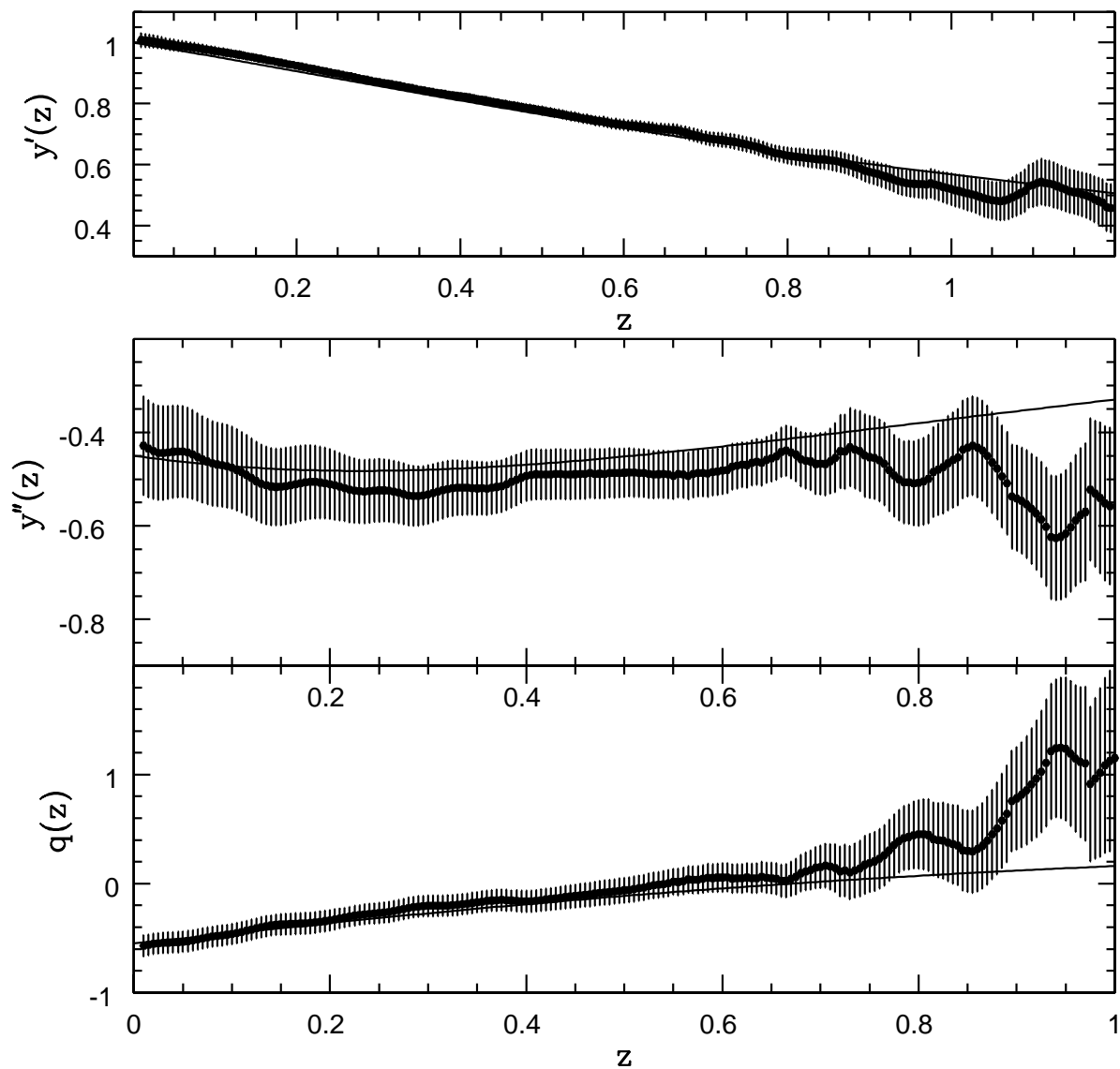


Fig. 18.— Results for  $y'(z)$ ,  $y''(z)$ , and  $q(z)$  obtained with the combined sample of 30 radio galaxies (solid circles), 192 supernovae (open circles), and 38 SZ clusters (stars), which is shown in Fig. 1. The solid curve illustrates the predicted value in a standard LCDM model with  $\Omega_m = 0.3$  and  $\Omega_\Lambda = 0.7$ .

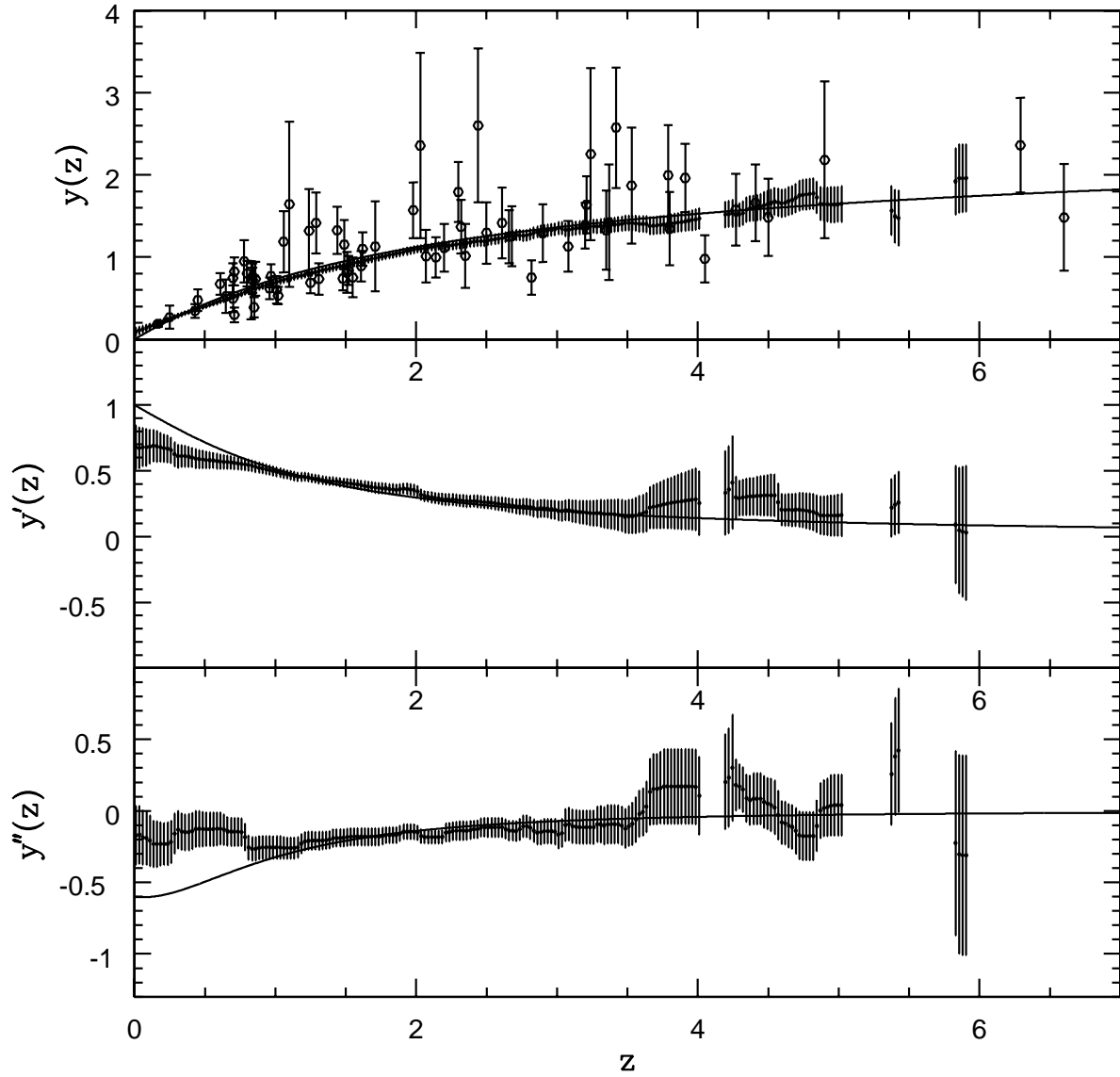


Fig. 19.— Results for  $y(z)$ ,  $y'(z)$ , and  $y''(z)$  obtained with the 69 gamma ray burst data of Schaefer (2007). The solid curve illustrates the predicted value in a standard LCDM model with  $\Omega_m = 0.4$  and  $\Omega_\Lambda = 0.6$ , which are the best fit values to this model obtained by Schaefer (2007).